Selected Problems in Strongly Correlated Electronic Models.

Thesis submitted for the degree of

"Doctor Philosophiæ"

CANDIDATE

Marco G. Airoldi

SUPERVISORS

Prof. Alberto Parola

Dr. Michele Fabrizio

Prof. Erio Tosatti

Dr. Giuseppe Santoro

October 1995

ACKNOWLEDGMENTS

My particular thanks go to Erio Tosatti, his suggestions and useful discussions have influenced every chapter of this thesis.

I am extremely grateful to Michele Fabrizio and Giuseppe Santoro for their valuable contribution and for interesting discussions. They made many comments and suggestions.

I am deeply indebted to Alberto Parola for his invaluable support and for discussing patiently, his helpful remarks and stimulating comments have led to many improvements to this thesis.

I would like also to thank S. Sorella for his helping, particularly during the work of the Hubbard model on the infinite dimensional diamond lattice, which becomes the first Chapter of this thesis.

Finally, I owe a debt of thanks to R. Valente for his helping with the LaTeX to edit the manuscript.

The stimulating atmosphere of ISAS (SISSA) has been essential in the realization of the work contained in this thesis, and I have a great debt toward my friends past and present.

Table of Contents

Table of Contents i

Introduction 1

Hubbard Model on the Infinite Dimensional Diamond Lattice 1

Correlated Electrons in a Lattice of Jahn–Teller Molecules. 6

Superconducting Ground State in a Model with Bond–Charge Interaction . 8

1 Hubbard Model on the Infinite Dimensional Diamond Lattice 13

1.1 Definitions and Mean-Field approximation 14

1.2 Momentum independence of the Self Energy 19

1.3 Reduction to a local problem 23

1.4 Numerical results 25

1.5 Phase diagram 30

2 Correlated Electrons in a Lattice of Jahn–Teller Molecules. 35

2.1 The molecule 35

2.2 Lattice of molecules 39

2.2.1 Weak coupling limit 39

2.2.2 Strong coupling limit 40

2.3 The two–particle solution and the low–density limit 43

2.3.1 Strong coupling limit, $g \to \infty$ 43

2.3.2 Weak coupling limit, $g \to 0$ 44

2.3.3 Two–particle bound state and the low–density limit 44

2.4 BCS-Mean Field Solution in the weak electron–phonon coupling regime . . 49

2.5 The E-e Jahn–Teller hamiltonian in the strong on site repulsion limit 51

3 Superconducting Ground State in a Model with Bond–Charge Interaction 57

3.1 The model and its symmetries 58

3.2 The two–particle problem 60

3.3 Two, three and four particle bound state in $D = 1$ 63

3.4 Correlation exponents in 1D: Zero–density limit 68

3.5 $D = 1$ at finite density 71

3.6 Mean Field Solution 75

3.7 Phase diagram 79

Conclusions 85

A $D = \infty$. Reduction to a local problem **89**

Bibliography **93**

Introduction

The discovery of high-T_c superconducting materials has revived interest in the physics of strongly–correlated electronic systems. In this thesis we present some studies on strongly correlated fermion model systems, concerning the problem of nonmagnetic metal - nonmagnetic insulator transition (known as the "Mott transition") in an infinite dimensional diamond lattice (Chapter 1) and the problem of modeling new mechanisms for the superconducting instabilities (Chapters 2 and 3).
In this Introduction, we would first like to introduce readers to broader issues and questions related to this work and anticipate some of the most relevant results obtained in the thesis.

Hubbard Model on the Infinite Dimensional Diamond Lattice

Theoretical investigations of correlated fermion systems are generally exceedingly difficult owing to the many–body nature of the problem. Even in its simplest formulation such as the single–band Hubbard model no one has given an exact solution, except in one dimension where there exist powerful techniques (Bethe–Ansatz, bosonization, etc.) which in many cases allow one to derive exact results. Unfortunately, these approaches are restricted to $D = 1$ and do not work in higher dimensions. By contrast, standard many–body perturbation techniques can be applied in all dimensions and in fact work generally better in

higher dimensions. In practice, however, they are limited to certain parameter ranges, e.g. very weak interactions, low densities etc. Alternatively one can resort to simpler methods, like mean field theories, slave boson approaches or variational methods which often provide valuable insight; nevertheless their actual validity is usually hard to estimate.

In view of the theoretical difficulties mentioned above it is of considerable help if one is at least able to obtain exact results for a model, even if oversimplified, in certain non trivial limits. If a solution is possible at all, it often turns out that perturbation techniques are able to connect this solution to more realistic parameter values.

In this respect the infinite dimensional limit of strongly correlated fermion systems has been the subject of large consideration in the recent past [1, 2, 3]. In classical statistical physics the limit of infinite spatial dimensions is well established, since it often allows for exact solutions. This is due to the fact that for $D \to \infty$ the number of nearest neighbors grows proportional to D, thus making fluctuations unimportant. As a consequence there is an intimate connection between solutions in $D = \infty$ and mean–field–type solutions. The same is basically true for quantum mechanical systems of localized spins. For example, in $D = \infty$ the Néel–state becomes the exact ground state of the Heisenberg model [4].

In a pioneering paper [1], Metzner and Vollhardt pointed out that the limit of large space dimensionality is also of great interest for systems with itinerant quantum mechanical degrees of freedom (e.g. fermionic lattice models), which simplify remarkably while retaining their main features, so that their physics remains non–trivial. Notice, however, that for itinerant Fermi systems, simple mean–field solutions, e.g. unrestricted Hartree–Fock, do not become exact in $D = \infty$. In fact, while the spatial fluctuations are frozen in $D = \infty$ and one–particle properties can thus be understood by looking at a single site of the lattice, the on–site quantum fluctuations (in imaginary time) are still present in infinite dimensions, making the problem non–trivial.

Nevertheless the limit of large spatial dimension leads to many simplifications in the theory. In particular it has been shown that diagrammatic treatments become very much simpler than in finite dimensions [1]. This property makes many problems, which are prohibitively

difficult in lower dimensions, tractable in $D = \infty$.

Finally the results obtained in $D = \infty$ can be extended to finite dimensions via systematic $1/D$ expansions [5, 6].

The Hubbard hamiltonian has certainly been the most studied fermion model in the infinite dimensional limit. As for the types of lattices which have been studied, recent investigations have focused on the hyper–cubic lattice at $D = \infty$ and on the Bethe lattice with infinite coordination number [7, 8, 9, 10]. In both cases the model can be exactly mapped onto a self-consistent one-impurity problem with a particular non-interacting density of states - gaussian, for the hyper-cubic case, semi-circular for the Bethe lattice case [7, 9, 10]. In this thesis (Chapter 1), we present an application of this technique to the ∞-dimensional generalization of the honeycomb ($D = 2$) or diamond ($D = 3$) lattices [11]. The common feature of this class of non–Bravais lattices, in any dimension $D \geq 2$, is a vanishing density of states (DOS) at the band center, $\rho(E) \propto |E|$, which results in a zero-gap semiconductor, or a zero-density semimetal, in the non-interacting case at exactly half filling. At $D = \infty$ the density of states becomes particularly simple, and reads: $\rho(E) = \frac{|E|}{t^2} e^{-E^2/2t^2}$, where t is a rescaled hopping parameter $t = \tilde{t}\,(2/D)^{-1/2}$ [a procedure which ensures that the kinetic energy does not trivially dominate as $D \to \infty$ (see Section 1.1)].

To fix the notation, we write the Hubbard hamiltonian as follows

$$H = -\tilde{t} \sum_{\mathbf{R} \in A, \{\mathbf{e}_i\}} \sum_{\sigma} \left[c^{+}_{\mathbf{R}+\mathbf{e}_i,\sigma}\, c_{\mathbf{R},\sigma} + h.c. \right] + U \sum_{\mathbf{R} \in A,B} n_{\mathbf{R},\uparrow}\, n_{\mathbf{R},\downarrow} \ ,$$

where the bipartite nature of the lattices under consideration allows us to identify two sublattices A and B, and $\{\mathbf{e}_i\}$ is a set of vectors connecting a site in A to its nearest-neighbors in B. In generalizing the honeycomb/diamond lattices to higher dimensions, we require that each site has $D + 1$ nearest-neighbors and that the angle θ between any two of the $D + 1$ vectors $\{\mathbf{e}_i\}$ is $\arccos(-D^{-1})$ (Section 1.1).

The infinite dimensional limit on a hyper–diamond lattice is studied by the well known mapping onto a self-consistent one-impurity problem. This is solved using Quantum Monte Carlo simulations and alternatively, second-order perturbation theory.

As in any half-filled bipartite lattice the model maps for $U \to \infty$ onto an unfrustrated Heisenberg model with antiferromagnetic (AF) nearest-neighbor coupling $J = 4\tilde{t}^2/U$, whose ground state has Néel AF long-range order. In the ordinary hyper-cubic case for $D \geq 2$, the Mean-Field (MF) critical value of U for the transition to a Néel antiferromagnet is actually vanishing ($U_c = 0$), because of perfect electron-hole nesting of the half-filled Fermi surface. By contrast, in the $D = \infty$ generalization of the honeycomb lattice, the Fermi surface is vanishingly small (more precisely, it is a $D-2$ dimensional object), the DOS at the Fermi level also vanishes as $\rho(E) \propto |E|$, and the MF value of U_c for the AF transition is pushed to a finite value $U_c > 0$ [12]. That this MF picture is qualitatively correct even in $D = 2$ is confirmed by the Quantum Monte Carlo (QMC) simulations for the honeycomb lattice [12]. In this case quantum fluctuations do increase the actual value of U_c, but only by about a factor 2: $U_c/\tilde{t} \approx 4.5$, whereas $U_c^{(MF)}/\tilde{t} = 2.23$ [12].

A finite value of U_c makes the situation interesting and potentially rich of surprises. First, there is a finite window of U-values near $U = 0$ where a nonmagnetic ground state should be stable. One may wonder if and what type of Fermi Liquid Theory is valid in that regime. Secondly, at half–filling, one can envisage the possibility of a (semi)metal-paramagnetic insulator (Brinkman–Rice) transition occurring at a lower U than that required for antiferromagnetism, in contrast to the MF picture. In $D = 2$ (honeycomb) the two transitions appeared to coincide as in the MF theory [12]. One of the motivations for the present study was the hope of clarifying, or confirming, some of these points, including the role of dimensionality and the possibility of a genuine (i.e., non magnetically driven) Mott-Hubbard transition, which is not yet found in any simple model.

The problem of the Mott transition is well known. In his pioneer work on the metal–insulator transition [13] Mott envisioned that in transition metals, as the Coulomb interaction among the charged carriers increases or as the interatomic spacing increases, the free motion of electrons in the lattice will cease at some point and the system will undergo a first order transition from a metal to an insulator. The first serious attempt to study this metal–insulator transition was due to Hubbard [14]. He based his calculation on

the "atomic" (zero–hopping) limit which naturally leads to a two–band picture, the lower (singly occupied) and upper (doubly occupied) Hubbard bands separated by the interaction U. He concluded that the metal–insulator transition occurs at a critical value U_c of order of the bandwidth, when the two bands stop overlapping. Although this picture leads to a metal insulator transition and provides a good insulating solution for large U, it fails to treat correctly the low energy physics in the metallic side: the Fermi liquid quasi–particles are absent. Brinkman and Rice (BR) [15] attacked the problem from the opposite limit by using a Gutzwiller variational wave function – a Fermi sea with double occupancy projected out – and found the metal–insulator transition at a much higher U_c. The Gutzwiller wave function gives a good Fermi liquid description for the metallic side, but misses the insulating side completely and lacks the high energy excitations which are the precursors, in the metal, of the upper and lower Hubbard bands of the insulating solution.

Although the Mott transition has acquired a much broader meaning over the years, it is still not clear what the right picture of the transition is, even in the simplest model which Hubbard treated in the early' 60s. In this respect the infinite dimensional limit makes the problem easier. In fact, in this limit, the Gutzwiller approximation used by BR to evaluate the energy of the Gutzwiller wave function becomes exact. Furthermore, it turns out that a major assumption made in the so-called Hubbard–III approximation [14], namely the self–energy being site diagonal, also becomes exact in infinite dimensions. Therefore, it is natural that a solution in the $D = \infty$ limit should provide a bridge between the Hubbard–III and the BR treatments and a clearer picture of the Mott transition.

In our study of the hyper–diamond lattice in $D = \infty$ we find that the transition is simultaneously metal–insulator and nonmagnetic-antiferromagnetic, i.e. the two transitions seem again to coincide as in $D = 2$. However, if we ignore the possibility of an antiferromagnetic solution, which sets in already for $U/t \approx 2.3$, we find a genuine "paramagnetic" Mott transition at $U/t \approx 8.5$. As in the hyper cubic case [9, 10, 16] this Mott-Hubbard transition would occur in a region of the phase diagram where the nonmagnetic solutions is unstable towards antiferromagnetism. It is therefore clear that the relevance of this genuine

Mott transition is again confined to models where disorder or some other frustrating agent destroys the antiferromagnetic order [17].

Correlated Electrons in a Lattice of Jahn–Teller Molecules.

Another interesting problem in the physics of strongly correlated electronic models is the interplay of orbital degeneracy and superconductivity in molecular conductors.

Generally, when atoms or molecules with orbitally degenerate valence levels are arranged to form a solid, the degeneracy of the isolated constituents is often broken, once the solid is formed. In many cases, in fact, the crystal field, produced by the surrounding atoms/molecules, is able to remove the original degeneracy. More importantly, kinetic energy broaders levels into bands, and this large bandwidth essentially "quenches" out the on–site orbital degeneracies. Yet, if the crystal symmetry is sufficiently high, and, more importantly, if electron hopping is sufficiently weak, the effects of orbital degeneracy may be far from being completely lifted. In this situation the molecular Jahn-Teller (JT) effect, arising from coupling electrons to on–site vibronic modes, may play an important role even in the solid. In particular it can induce a global symmetry–lowering lattice deformation lifting the residual degeneracy ("static" Jahn-Teller effect). This is the case for the so–called "cooperative" Jahn–Teller systems [18]. However if the phonon frequencies are high in comparison with the electron hopping, the static distortion may become disadvantageous and the original symmetry may be recovered dynamically ("dynamic" Jahn-Teller effect). A primary and well known consequence of the dynamic mixing between electronic and vibronic degrees of freedom, is the renormalization of several electronic matrix elements by the so-called Ham reduction factor [19]. Apart from this suppression factor, other interesting properties may arise when dynamical JT effect is important.

For instance, in the context of superconductivity in fullerenes, it has been recently proposed [20] that the dynamical JT effect may be associated with an increase of the electronic

pairing interaction. In the specific case of charged fullerene molecules, the JT effect arises mainly from coupling the partially occupied t_{1u} orbitals with the H_g vibronic modes, even though for a realistic description one has to take into account other modes such as A_g [21, 22] and other orbitals, such as h_u and t_{1g}. Since the detailed physical model of C_{60} is very complicated, in Ref. [23] a simplified version was introduced, aimed at capturing the essential physics of the problem. The model consists of a lattice of molecules, each with two (instead of three) degenerate orbitals coupled to a doubly-degenerate (instead of five–fold degenerate) vibronic mode. The hamiltonian of each molecule is now described by a so-called E–e JT hamiltonian, which is the simplest case of dynamic JT effect [18]. In spite of its simplicity, the lattice of E–e molecules exhibits rather striking and unexpected features [23, 24, 25]. In particular it was found that, besides the usual polaronic attraction, a new type of electron pair binding mechanism is present in the model.

Besides the application to C_{60}, the doubly degenerate Jahn-Teller model might provide some useful informations for other systems where the Jahn–Teller effect is expected to be important, such as compounds containing magnetic ions with unfilled d or f shells. In this case it is well known that the interplay between the Jahn–Teller effect and the strong electronic correlations plays a very important role in determining both the structural and the magnetic properties (Section 2.5). For a review mainly on transition metal compounds see e.g. Ref. [18] and Ref. [26], and for rare earth compounds see Ref. [27]. A typical example where the doubly degenerate JT model could be relevant is a transition metal ion, whose valence state is five–fold orbitally degenerate. In cubic symmetry, the crystal field splits the d-levels into a three–fold degenerate t_{2g} level and a two–fold degenerate e_g. Exactly for a tetrahedral distortion, the two–fold degenerate e_g is the ground state.

In this thesis we study the lattice of E–e molecules both in the weak and in the strong electron–phonon coupling limit.
We show that the orbital degeneracy induces an intersite pairing mechanism absent in the standard non–degenerate polaronic model. This effect can lead to a superconducting ground

state even if the Coulomb repulsion between electrons overcomes the polaronic attraction. The model is solved exactly for two particles both in the strong and in the weak electron–phonon coupling limit and it is shown that, even if the polaronic attraction is disregarded, two electrons in the vacuum, for $D = 1$ and 2, still bind with a binding energy proportional to the effective hopping (the bare hopping reduced by the Ham factor). The presence of such a zero–density bound state for two particles although in itself not relevant to the finite density case suggests that, at low density and low dimensionality ($D = 1, 2$), superconductivity is due to condensation of pre–existing pairs (dimers).

In order to determine the phase diagram of the system also at finite density we have analyzed the weak electron–phonon coupling limit of the model within a BCS mean field approach. We found that the correlated hopping, induced by the Jahn–Teller coupling, favors the superconductivity [25]. This new pairing mechanism, which is absent in the non–degenerate polaronic model, is not easily destroyed by a repulsive U, it is more effective at low carrier density, and is apparently immune from the polaron mass increase with self–trapping, which depresses T_c in strongly coupled electron–phonon systems [23, 24, 25]. Another interesting feature of this model in one dimension, at least at sufficiently strong electron–phonon interaction, is the presence of a spin gap both in the superconducting region and in the normal state which is obtained by increasing U [24, 28]. An open question is whether this spin gap is preserved also in higher dimensions or if it is instead specific of 1D.

Superconducting Ground State in a Model with Bond–Charge Interaction

In the last Chapter of my thesis I discuss another type of mechanism purely electronic, for the superconducting instabilities in strongly correlated electronic systems. This is a highly challenging issue after the discovery of high temperature cuprate superconductors. Several models have been proposed in order to describe the essential physics of these systems and

in particular Hubbard–type models have been the subject of a large consideration in the recent past. It has soon become clear that superconductivity in purely electronic $1D$ and $2D$ systems can be induced by direct (*diagonal*) interactions, as in the extended Hubbard model (with $V > 0$) or in the $t - J$ model at sufficiently large J. This mechanism is rather insensitive to dimensionality and, although off diagonal long range order cannot be achieved in one dimension, clear signals of a superconducting instability are present also in 1D models [29, 30]. A serious drawback of this type of mechanism however is the presence of (at least) another instability leading to either CDW's or phase separation, which occurs just nearby the superconducting region in systems with non–zero range interactions. A very unlikely fine–tuning of the parameters in the hamiltonian is needed to obtain superconductivity without CDW's or phase separation [31]. The physical reason for the proximity of the two instabilities can be traced back to the essentially *classical* (density–density or spin–spin) character of the interaction which generates superconductivity. If this interaction becomes sufficiently strong, it overcomes the kinetic energy term and favors the state which minimizes the potential energy, giving rise to phase separation.

A different type of *non–classical* interaction leading to superconductivity without other instabilities [32] is the so called bond–charge interaction, which will be investigated in Chapter 3.

This term describes the modification of the electron hopping by the presence of other spectator electrons on the sites involved in the hopping process. The simplest hamiltonian, which describes the model, can be written as:

$$\begin{aligned} H &= -t \sum_{<rr'>} \sum_{\sigma} \left(c^{\dagger}_{r\sigma} c_{r'\sigma} + h.c. \right) + U \sum_{r} n_{r\uparrow}\, n_{r\downarrow} \\ &+ \gamma \sum_{<rr'>} \sum_{\sigma} \left(c^{\dagger}_{r\sigma} c_{r'\sigma} + h.c. \right) \left(n_{r'-\sigma} + n_{r-\sigma} \right) , \end{aligned}$$

where the second term is the usual Hubbard repulsive interaction and the last term represents the bond–charge interaction. In Chapter 3 we will consider an hamiltonian which is a little bit more general of that written above.

All recently proposed integrable models of strongly correlated electrons, showing super-

conducting instabilities in the presence of repulsive interaction, contain as the essential part the bond–charge interaction [33, 34]. For instance, the supersymmetric extended Hubbard model proposed by Essler, Korepin and Schoutens [33] (EKS–model) contains, in addition to the usual Hubbard term and nearest–neighbour density–density interactions, the bond–charge term as well as the spin–spin interaction and the pair–hopping term. Unfortunately, the symmetry conditions ensuring integrability, impose a strong restriction on the values of the coupling constants of the model and leave, besides the Hubbard coupling constant U, only a single free parameter in the theory. This severe restriction makes it difficult to distinguish the contribution coming from the different terms and to recognize the one which is responsible for superconductivity.

It's therefore of great interest to study the different correlation mechanisms separately. We will focus our attention on the bond–charge interaction and on the role played by this term as a source of superconductivity.

The bond–charge interaction, as a source of superconducting instabilities in high–T_c oxides, was first discussed by Hirsch and Marsiglio in a series of papers [35, 36, 37, 38]. These authors pointed out, using a standard BCS type mean–field approach, that the bond–charge interaction produces an effective attraction with a strong band–filling dependence, which is one of the challenging properties of the high–T_c superconducting materials.

On the other hand, although at first sight this type of interaction seems artificial, it emerges rather naturally in the construction of a tight binding hamiltonian [39, 40, 41]. In the standard case of Coulomb repulsion all model parameters in H are positive. This means that the correlation effect, produced by the bond–charge term, is more attractive in the limit of low hole concentration (i.e. when the Fermi level is close to the top of the band). Moreover the bond–charge interaction can naturally be thought of as the result of a trace over additional degrees of freedom either electronic or of different physical origin [24, 42, 43, 44, 45, 46]. For instance, in connection with the problem discussed in Chapter 2, the bond–charge hamiltonian can be obtained as an effective non–degenerate electronic hamiltonian for the E–e Jahn–Teller model by integrating out the degrees of freedom associated to the orbital

degeneracy (see Section 3.2). In such a case the sign in front of the bond–charge term is negative ($\gamma < 0$), which reflects to a tendency to pairing electrons instead of holes.

In Chapter 3 we will take such a bond–charge model as an effective electronic model without entering in a discussion about the physical origin of the interaction. The emphasis of our investigation will be on the properties of these systems and on the resulting zero temperature phase diagram both in one and two dimensions. In particular, we will show, by use of analytical as well as numerical techniques, that in a wide parameter region the model has a superconducting ground state [47]. Superconductivity is robust to the presence of local repulsion U due to the off diagonal nature of the bond–charge interaction. The character of the Cooper pair changes with density, at fixed interaction strength, going from real space dimers at low density to less strongly bound pairs largely overlapping when density is increased. The analysis of the model can be made fully quantitative in 1D because of the extremely powerful techniques available in one dimensional systems: bosonization, conformal field theory and weak coupling renormalization group which can be successfully supplemented by numerical methods. The 1D phase diagram shows a transition, which is quantitatively characterized, as the repulsion U is decreased, between a Luttinger liquid and a strong coupling phase with diverging superconducting susceptibility. In 2D, the low density part of the phase diagram can be obtained exactly, while overall numerical diagonalizations at quarter filling qualitatively support a mean field approximation. The 2D phase diagram is qualitatively similar to the 1D case: a ground state with spin gap and off-diagonal long range order at small positive U and a Fermi liquid with no sign of phase separation at larger U.

1 Hubbard Model on the Infinite Dimensional Diamond Lattice

The study of interacting fermionic lattice models in the limit of large spatial dimension has been the subject of a rapidly growing attention in the recent past [1].

In this Chapter, we present and study the infinite dimensional limit of the Hubbard model on a class of non-nested bipartite lattices which generalize the two-dimensional honeycomb and the three-dimensional diamond lattice, and are characterized by a semi-metallic non-interacting density of states [11].

The definition of the hyper–diamond lattice in D dimensions is presented in Section 1.1, where we provide also a mean field treatment of the problem.

The essence of our approach to the $D = \infty$ limit of this class of models is very similar to those already appeared in the literature, and is discussed, for completeness, in Sections 1.2 and 1.3. It suffices here to say that a mapping into a self-consistent Anderson impurity problem [7] allows us to calculate the local Green's function in a quite reliable way, by either a one-impurity Quantum Monte Carlo simulation or a surprisingly good perturbative approach.

Single particle properties are straightforwardly obtained from the Green's function (Section 1.4).

Finally in Section 1.5 we discuss the phase diagram of the model at half–filling.

1.1 Definitions and Mean-Field approximation

The hyper-diamond lattice in D dimensions can be defined as a bipartite lattice satisfying the following two conditions:

- Each point in the lattice has $D+1$ nearest neighbors at a distance a (which we take hereafter to set the unit of length, $a=1$), belonging to the opposite sublattice.
- Denoting by $\{\mathbf{e}^i\}_D$ the set of $D+1$ unit vectors connecting a point of the lattice to its nearest neighbors, the angle between any two vectors $\mathbf{e}^i$ and $\mathbf{e}^j$ is a constant:

$$\mathbf{e}^i \cdot \mathbf{e}^j = \alpha_D \qquad\qquad \forall i \neq j \ . \tag{1.1}$$

This definition reduces, for instance, to the honeycomb lattice for $D=2$ ($\alpha_2 = -\frac{1}{2} = \cos 120^o$). For $D=3$ it coincides with the diamond lattice ($\alpha_3 = -\frac{1}{3} \approx \cos 109^o$). We will show that the constant α_D is given, in any dimension, by $\alpha_D = -\frac{1}{D}$.

Proof. (By induction). Suppose that $\{\tilde{\mathbf{e}}^i\}_{D-1}$ is a set of D unit vectors in $D-1$ dimensions satisfying the condition (1.1). We will now construct the required set of vectors $\{\mathbf{e}^i\}_D$ in D dimensions as follows:

$$\begin{aligned} \mathbf{e}^i &= (\gamma\, \tilde{\mathbf{e}}^i, \alpha_D) \qquad\qquad i = 1,2,...,D \\ \mathbf{e}^{D+1} &= \underbrace{(0,0,0,0,\cdots,0,1)}_{D} \end{aligned} \tag{1.2}$$

where the first $D-1$ components of each vector $\mathbf{e}^i$ ($i=1,2,...,D$) coincide with the corresponding components of $\tilde{\mathbf{e}}^i$ scaled by a common factor γ, the last component being equal to α_D. Simple algebra shows that the condition (1.1) is verified and the vectors $\mathbf{e}^i$ are normalized to one, provided we require:

$$\begin{aligned} \gamma &= \sqrt{1-\alpha_D^2} \\ \alpha_D &= \frac{\alpha_{D-1}}{1-\alpha_{D-1}} \ . \end{aligned} \tag{1.3}$$

It is now easy to verify, by direct substitution, that $\alpha_D = -\frac{1}{D}$ is the only solution of Eq. (1.3) with initial condition $\alpha_{D=2} = \cos 120^o$, which completes the proof.

This proof provides also an iterative method to construct the set of vectors $\{\mathbf{e}^i\}_D$ in D dimensions. One can even start from $D = 1$ where the hyper-diamond degenerates into:

$$\{\mathbf{e}^i\}_{D=1} = \{\mathbf{e}^1 = (1)\,,\ \mathbf{e}^2 = (-1)\}\,, \tag{1.4}$$

and construct lattices of higher dimension using Eqs. (1.2) and (1.3) (see Fig. 1.1).

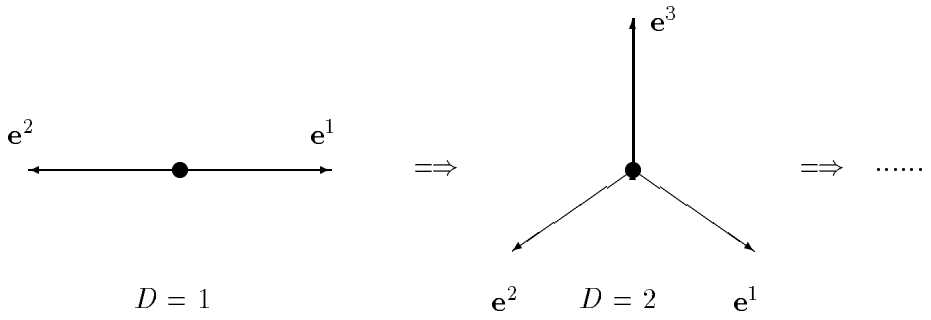

Figure 1.1: Iterative method to construct the hyper–diamond lattices starting from $D = 1$.

Note, in passing, that the vectors $\{\mathbf{e}^i\}_D$ become orthogonal as $D \to \infty$.

In D dimensions, the unitary cell is defined by the vectors:

$$\mathbf{a}_i = \mathbf{e}^{D+1} - \mathbf{e}^i \qquad\qquad i = 1, 2, ..., D \tag{1.5}$$

and the reciprocal basis vectors are defined by the relation $\mathbf{a}_i \cdot \mathbf{b}_j = 2\pi\delta_{ij}$.
The Hubbard hamiltonian on this class of bipartite lattices can be written as:

$$H = -\tilde{t} \sum_{\mathbf{R}\in A, \mathbf{e}^i} \sum_{\sigma} [c^+_{\mathbf{R},\sigma}\, c_{\mathbf{R}+\mathbf{e}^i,\sigma} + h.c.] + U \sum_{\mathbf{R}\in A \bigoplus B} n_{\mathbf{R},\uparrow}\, n_{\mathbf{R},\downarrow} \tag{1.6}$$

where $\mathbf{R}$ stands for a generic site of sublattice A, and $\mathbf{e}^i$ indicates any of the $D+1$ vectors connecting a site in A to its nearest-neighbors in B. ($n_{\mathbf{R},\sigma} = c^+_{\mathbf{R},\sigma}\ c_{\mathbf{R},\sigma}$ is the number operator).

In order to derive the density of states in the limit of large spatial dimension we have to diagonalize the Hubbard hamiltonian (1.6) for $U = 0$. We first revert from Wannier states to Bloch waves:

$$c^+_{A\mathbf{k},\sigma} = \frac{1}{\sqrt{N}} \sum_{\mathbf{R}\in A} e^{-i\ \mathbf{k}\cdot\mathbf{R}} c^+_{\mathbf{R},\sigma} \tag{1.7}$$

$$c^+_{B\mathbf{k},\sigma} = \frac{1}{\sqrt{N}} \sum_{\mathbf{R}\in A} e^{-i\ \mathbf{k}\cdot(\mathbf{R}+\mathbf{d})} \cdot c^+_{\mathbf{R}+\mathbf{d},\sigma}\ , \tag{1.8}$$

where N is the number of lattice cells, and $\mathbf{d} = \mathbf{e}^{D+1}$. Using this transformation the hamiltonian becomes partially diagonal (A and B operators are still coupled) and reads:

$$H_{U=0} = -t \sum_{\mathbf{k}}^{BZ} [F_{\mathbf{k}}\ c^+_{A\mathbf{k},\sigma}\ c_{B\mathbf{k},\sigma} + F^*_{\mathbf{k}}\ c^+_{B\mathbf{k},\sigma}\ c_{A\mathbf{k},\sigma}]\ , \tag{1.9}$$

where the sum over $\mathbf{k}$ runs over the first Brillouin zone, and

$$F_{\mathbf{k}} = \sum_{j=1}^{D+1} e^{-i\ \mathbf{k}\cdot\mathbf{e}^j}\ . \tag{1.10}$$

The diagonalization of $H_{U=0}$ is then carried out by defining a new set of creation and destruction operators: ($n = 1, 2$)

$$\psi_{n\mathbf{k},\sigma} \quad = \quad u_{n\mathbf{k}}\ c_{A\mathbf{k},\sigma} + v_{n\mathbf{k}}\ c_{B\mathbf{k},\sigma}\ , \tag{1.11}$$

where the coefficients are subject to the canonicity restriction $|u_{n\mathbf{k}}|^2 + |v_{n\mathbf{k}}|^2 = 1$, and selected in such a way as to put $H_{U=0}$ in the form:

$$H_{U=0} = \sum_{\mathbf{k}}^{BZ} \sum_{n,\sigma} E_{n\mathbf{k}}\ \psi^+_{n\mathbf{k},\sigma}\ \psi_{n\mathbf{k},\sigma}\ . \tag{1.12}$$

The band energies $E_{n\mathbf{k}}$ turn out to be given by

$$E_{n\mathbf{k}} = \pm\tilde{t}\ \mid F_{\mathbf{k}} \mid\ , \tag{1.13}$$

which, expressing the momentum as $\mathbf{k} = \sum_j k_j \mathbf{b}_j$, can be rewritten in the form

$$|E_{n\mathbf{k}}| \ = \ \tilde{t}\ |F_{\mathbf{k}}| \ = \ \tilde{t}\ |1 + \sum_{j=1}^{D} e^{i\ 2\pi k_j}| \ = \ \sqrt{X^2 + Y^2} \qquad\qquad k_j \in (0,1)\ , \tag{1.14}$$

X and Y being defined by

$$X = \tilde{t}\left(1+\sum_{j=1}^{D}\cos 2\pi k_j\right) \tag{1.15}$$
$$Y = \tilde{t}\sum_{j=1}^{D}\sin 2\pi k_j \ .$$

The crucial step is now to apply the central limit theorem to Eq. (1.15). The probability distributions for the variables X and Y become gaussians in the limit of large dimension and are given by

$$P_X(X) = \frac{1}{\sqrt{\pi\ \tilde{t}^2\ D}}\ e^{-\frac{(X-\tilde{t})^2}{\tilde{t}^2\ D}} \tag{1.16}$$
$$P_Y(Y) = \frac{1}{\sqrt{\pi\ \tilde{t}^2\ D}}\ e^{-\frac{Y^2}{\tilde{t}^2\ D}}\ . \tag{1.17}$$

It is then clear that, in order to obtain a model having a non trivial limit for $D\to\infty$, the parameter $\tilde{t}$ in the kinetic energy must be scaled so as to make the variance of the distributions P_X and P_Y equal to a finite non-vanishing constant t at $D=\infty$, i.e.

$$\tilde{t} = \sqrt{\frac{2}{D}}\ t\ . \tag{1.18}$$

Rewriting $\tilde{t}$ in terms of t and sending $D\to\infty$, we get that the limiting distributions for X and Y actually coincide ($P_X = P_Y = P$),

$$P(X) = \frac{1}{\sqrt{2\pi\ t^2}}\ e^{-\frac{X^2}{2\,t^2}}\ , \tag{1.19}$$

and the distribution for the energy (i.e. the density of states) becomes:

$$\rho(E) = \int dX\,dY\ P(X)\,P(Y)\,\delta(E-\sqrt{X^2+Y^2}) = \frac{|E|}{t^2}\ e^{-\frac{E^2}{2\,t^2}}\ . \tag{1.20}$$

Notice that the density of states goes to zero for $E\to 0$.

A comparison between ρ in $D=2,3$ and in $D=\infty$ is shown in Fig. 1.2.

We will now give a brief account of the mean-field treatment of the full Hubbard Hamiltonian on the hyper–diamond lattice. The Hartree-Fock mean field theory can be obtained by approximating the exact interaction operator in Eq. (1.6), as a bilinear form:

$$H_{int} = U\sum_{\mathbf{R}\in A\bigoplus B}\langle n_{\mathbf{R},\uparrow}\rangle\ n_{\mathbf{R},\downarrow} + n_{\mathbf{R},\uparrow}\ \langle n_{\mathbf{R},\downarrow}\rangle\ , \tag{1.21}$$

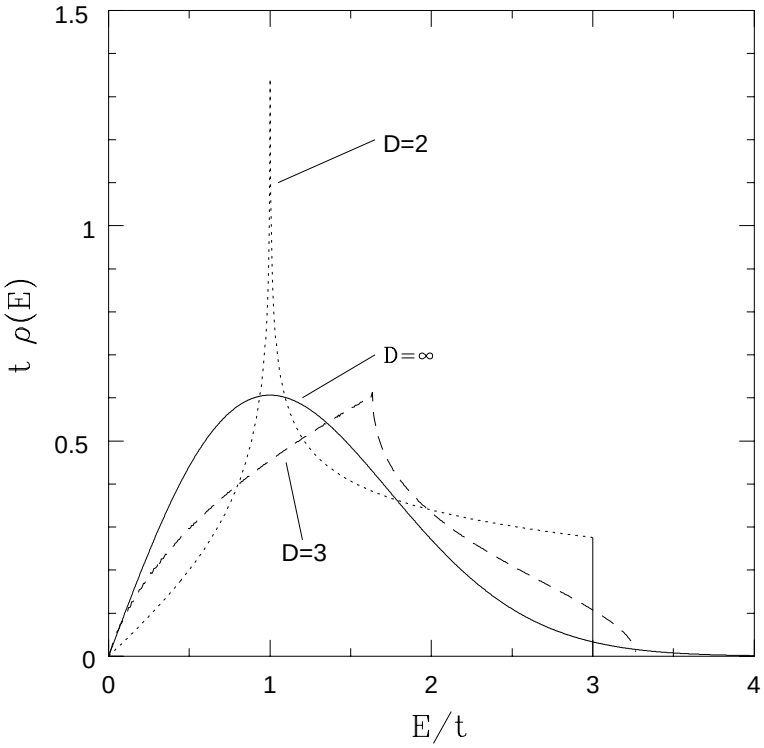

Figure 1.2: Comparison between the non-interacting density of states for the honeycomb ($D = 2$) and diamond ($D = 3$) lattices, and the $D = \infty$ result. t is a rescaled hopping parameter $t = (2/D)^{-1/2}\tilde{t}$.

where the averages $\langle n_{\mathbf{R},\sigma} \rangle$ have to be determined self-consistently. To study a Néel–type of antiferromagnetic long-range order at half filling, the choice $\langle n_{\mathbf{R},\sigma} \rangle = \frac{1}{2} + (-1)^R \, \sigma \, \frac{M}{2}$ is made, where the notation $(-1)^R$ stands for $+1$ on sublattice A and -1 on B. It is easy to demonstrate that, within this approximation, the system has a gap Δ which is related to U by the equation:

$$U \int_0^\infty dE \; \rho(E) \, \frac{1}{\sqrt{E^2 + \Delta^2}} \; \tanh\left(\frac{\beta}{2} \sqrt{E^2 + \Delta^2}\right) = 1 \, , \tag{1.22}$$

where $\beta = \frac{1}{T}$, and T is the temperature. The critical value U_c of the interaction U which determines the transition between the paramagnetic-metallic phase ($\Delta = 0$) and

antiferromagnetic-insulating phase is therefore defined by:

$$U_c \int_0^\infty dE\ \rho(E)\frac{1}{|E|}\ \tanh(\frac{\beta}{2}\,|E|)\ = 1 \tag{1.23}$$

which is easily calculated at $T = 0$, giving:

$$\frac{U_c}{t}(T=0) = \frac{4}{\sqrt{2\ \pi}} \approx 1.596\,. \tag{1.24}$$

When U is less than U_c, the system is paramagnetic and semimetallic ($\Delta = 0$) while for U larger than U_c the system becomes antiferromagnetic and insulating.

In the next two sections we will give some technical details on the method used to study the model.

1.2 Momentum independence of the Self Energy

A crucial simplification of the Hubbard model at $D = \infty$ consists in the fact that the self-energy function Σ becomes site-diagonal, a property which can be proved using the methods of Ref. [48] with minor modifications due to the presence of phase-factors in the off-diagonal Green's functions. More precisely, we will first consider the behavior of the non-interacting Green's function $G^o_{\alpha\beta}(i,j)$ for $D \to \infty$, the symbol α (β) stands for the sublattice to which site i (j) belongs. The Green's function $G^o_{\alpha\beta}(i,j)$ can be expressed in terms of its Fourier transform by the relation:

$$G^o_{\alpha\beta}(\mathbf{R} = \mathbf{R}_i - \mathbf{R}_j \in A, \omega) = \int_{BZ} \frac{d^D\mathbf{k}}{(2\pi)^D} e^{i\,\mathbf{k}\cdot\mathbf{R}}\ G^o_{\alpha\beta}(\mathbf{k},\omega) \tag{1.25}$$

where $G^o_{\alpha\beta}$ are given by the relations:

$$G^o_{AA}(\mathbf{k},\omega) = G^o_{BB}(\mathbf{k},\omega) = \frac{1}{2}\,[G^o_1(\mathbf{k},\omega) + G^o_2(\mathbf{k},\omega)] \tag{1.26}$$

$$G^o_{AB}(\mathbf{k},\omega) = e^{i\,\phi_{\mathbf{k}}}\,\frac{1}{2}\,[G^o_1(\mathbf{k},\omega) - G^o_2(\mathbf{k},\omega)] \tag{1.27}$$

$$G^o_{BA}(\mathbf{k},\omega) = e^{-i\,\phi_{\mathbf{k}}}\,\frac{1}{2}\,[G^o_1(\mathbf{k},\omega) - G^o_2(\mathbf{k},\omega)] \tag{1.28}$$

with:

$$G_i^o(\mathbf{k},\omega) = \frac{1}{i\,\omega + \mu - E_i(\mathbf{k})} \qquad\qquad e^{i\,\phi_{\mathbf{k}}} = \frac{F_{\mathbf{k}}}{|F_{\mathbf{k}}|} \tag{1.29}$$

and $E_1(\mathbf{k}) = -t\,|F_{\mathbf{k}}|$, $E_2(\mathbf{k}) = t\,|F_{\mathbf{k}}|$. We will first consider the component $G^o_{AA}(\mathbf{R},\omega)$ of the Green's function. Due to the fact that $G^o_{AA}(\mathbf{k},\omega)$ depends on $\mathbf{k}$ only through $E(\mathbf{k})$, it is possible to incorporate the momentum integration in the function:

$$v^{AA}_{\mathbf{R}}(E) = \int_{BZ} \frac{d^D\mathbf{k}}{(2\pi)^D}\,\delta(E - E_{\mathbf{k}})\,e^{i\,\mathbf{k}\cdot\mathbf{R}}\ , \tag{1.30}$$

in terms of which Eq. (1.25) reads:

$$G^o_{AA} = \int dE\ v^{AA}_{\mathbf{R}}(E)\,G^o_{AA}(E,\omega)\ . \tag{1.31}$$

The behavior of $v^{AA}_{\mathbf{R}}$ can be analyzed by taking the Fourier transform with respect to E

$$\Psi_{\mathbf{R}}(s) = \int dE\ e^{i\,s\,E}\ v^{AA}_{\mathbf{R}}(E) = \int_{BZ} \frac{d^D\mathbf{k}}{(2\pi)^D}\,e^{i\,(s\,E(\mathbf{k}) + \mathbf{k}\cdot\mathbf{R})}\ . \tag{1.32}$$

Clearly, for $\mathbf{R} = 0$, $\Psi_{\mathbf{R}}(s)$ becomes the Fourier transform of the density of state $\rho(E)$, while for any other value of $\mathbf{R}$ belonging to sublattice A, it vanishes like $1/D$ or faster in the limit of infinite dimension. In fact, when $\mathbf{R}$ is a nearest-neighbor (in A) of the lattice point $\mathbf{R} = 0$, $\Psi_{\mathbf{R}}(s)$ can be rewritten as:

$$\begin{aligned}
\Psi_{\mathbf{R}=\mathbf{a}^j}(s) &= \int_{BZ} \frac{d^D\mathbf{k}}{(2\pi)^D}\,e^{i\,s\,E(\mathbf{k})}\,e^{i\,2\pi k_j} \\
&= \frac{1}{D}\int_{BZ} \frac{d^D\mathbf{k}}{(2\pi)^D}\,e^{i\,s\,E(\mathbf{k})}\sum_{j=1}^{D} e^{i\,2\pi k_j} \\
&= \frac{1}{D}\int_{BZ} \frac{d^D\mathbf{k}}{(2\pi)^D}\,e^{i\,s\,E(\mathbf{k})}\left[\frac{\sqrt{D}}{\sqrt{2}t}\,(X + iY) - 1\right]\ ,
\end{aligned} \tag{1.33}$$

where the variables X and Y have been introduced in Section 1.1, and t is the scaled hopping parameter. Introducing, in the limit of $D \to \infty$, the gaussian distributions $P(X)$ and $P(Y)$ in the integral, we can rewrite:

$$\begin{aligned}
\Psi_{\mathbf{R}=\mathbf{a}^j}(s) &= \frac{1}{D}\int_{-\infty}^{+\infty} dX\,dY\,P(X)\,P(Y)\,e^{i\,s\,\sqrt{X^2+Y^2}}\left[\frac{\sqrt{D}}{\sqrt{2}t}\,(X + iY) - 1\right] \\
&\approx \text{const}\ O(\frac{1}{D})\ ,
\end{aligned} \tag{1.34}$$

since the integral of the $(X + iY)$ term vanishes by parity.

The main consequence of this result is that the Green's function $G^o_{AA}(\mathbf{R},\omega)$ for $D \to \infty$ can be expressed as:

$$G^o_{AA}(\mathbf{R},\omega) = \delta_{\mathbf{R},0}\, G^o_{AA}(\omega) \,+\, O(\frac{1}{D})\,. \tag{1.35}$$

It is important to note that the $\mathbf{R} \neq 0$ terms in the Green's function $G^o_{AA}(\mathbf{R},\omega)$ can turn out to be non negligible anywhere there is a sum over $\mathbf{R}$ because, in this case, factors of $1/D$ can be compensated by the sum, giving a finite result. (For instance, the inverse-Fourier transform of Eq. (1.35), which is the non-interacting Green's function $G^o_{AA}(\mathbf{k},\omega)$ in momentum space, depends on the momentum $\mathbf{k}$).

The previous demonstration can be repeated, with some little modification, also for the off-diagonal component G^o_{AB} of the Green's function. In this case, G^o_{AB} depends of the momentum $\mathbf{k}$ through the energy $E(\mathbf{k})$ and the phase-factor $\phi_{\mathbf{k}}$. The corresponding function $v^{AB}_{\mathbf{R}}$ is then given by:

$$v^{AB}_{\mathbf{R}}(E) = \int_{BZ} \frac{d^D\mathbf{k}}{(2\pi)^D}\, \delta(E - E_{\mathbf{k}})\, e^{\,i\,(\mathbf{k}\cdot\mathbf{R} + \phi_{\mathbf{k}})} \tag{1.36}$$

and its Fourier transform reads:

$$\Psi_{\mathbf{R}}(s) = \int_{BZ} \frac{d^D\mathbf{k}}{(2\pi)^D}\, e^{\,i\,(s\,E(\mathbf{k}) + \mathbf{k}\cdot\mathbf{R} + \phi_{\mathbf{k}})}\,. \tag{1.37}$$

The value of $\Psi_{\mathbf{R}}(s)$ for a nearest-neighbor site, i.e., $\mathbf{R} = 0$ (recall that $\mathbf{R}$ in our notation is the cell variable), is given by:

$$\Psi_{\mathbf{R}=0}(s) = \int_{BZ} \frac{d^D\mathbf{k}}{(2\pi)^D}\, e^{\,i\,s\,E(\mathbf{k})}\, e^{i\phi_{\mathbf{k}}} \;\approx\; \text{const}\, O(\frac{1}{\sqrt{D}})\,, \tag{1.38}$$

where steps similar to the ones used to arrive at Eq. (1.34) have been made. In a similar way one can show that every non site-diagonal term in (G^o_{AB}, G^o_{AB}) vanishes at least as $1/\sqrt{D}$ for $D \to \infty$.

Using the previous result, we can now analyze the locality property of the self-energy in $D = \infty$. We will consider only the second order diagram in U, but the argument can be

easily generalized to all orders in U with a little effort. The second order contribution to the self energy is represented by the diagram in Fig. 1.3. The analytic expression associated

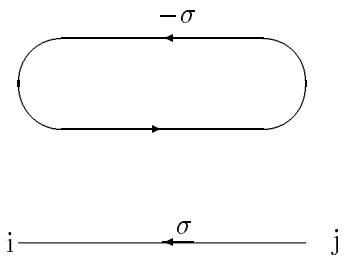

Figure 1.3: Second–order contribution to the self energy $\Sigma_{\alpha\beta}(i,j)$.

with this diagram is (the label α and β denote sublattice A or B):

$$\Sigma_{\alpha\beta}(i,j)(\tau) = G^o_{\alpha\beta}(i,j)(\tau)\, G^o_{\alpha\beta}(i,j)(\tau)\, G^o_{\beta\alpha}(j,i)(\tau) = \delta_{ij}\, \Sigma_{\alpha\beta}(i,i)(\tau) + O(\frac{1}{D^{3/2}}) \quad (1.39)$$

and the corresponding Fourier transform is given by:

$$\Sigma_{\alpha\beta}(\mathbf{k},\omega) = \sum_{\mathbf{R}\in A} \int d\tau\, e^{i\omega\tau} e^{-i\,\mathbf{k}\cdot\mathbf{R}}\, \Sigma_{\alpha\beta}(i,j)(\tau) = \Sigma_{\alpha\beta}(\omega) + O(\frac{1}{D^{1/2}})\,. \quad (1.40)$$

A similar argument can be applied to any n-th order *irreducible* self-energy diagram. In this case, $n-2$ internal lattice-site sums together with $2n-1$ internal G^o-lines conspire to make the formal leading correction to the momentum independence of order $1/\sqrt{D}$, as in Eq. (1.40). Thus the self-energy becomes local (i.e., momentum independent) for $D=\infty$, a property which introduces a considerable simplification in the theory.

Note, finally, that the independence of the momentum $\mathbf{k}$ is true only for an irreducible diagram. To appreciate why this is so, consider, for instance, the reducible fourth-order diagram in Fig. 1.4. Formally, this diagram has $2n-2=2$ internal site sums and $2n-1=7$ internal lines, exactly as a fourth order irreducible diagram. In this case, however, we can write the double sum over the internal vertex k and l in terms of lower order irreducible self-energy diagrams as follows:

$$[\text{Reducible Diagram}] = \sum_{k,l} \Sigma^{(2)}(i,k)\, G^o(k,l)\, \Sigma^{(2)}(l,j)\,. \quad (1.41)$$

Figure 1.4: Reducible fourth–order diagram.

If we consider, in this sum, the term which corresponds to the labels $k = i$ and $l = j$ we obtain, for $i \neq j$, the contribution:

$$[\text{Term with } k = i, l = j] \;=\; \Sigma^{(2)}(i,i)\, G^{o}(i,j)\, \Sigma^{(2)}(j,j) \;\approx\; O(\frac{1}{\sqrt{D}})\,, \tag{1.42}$$

which is non-negligible when transformed back in momentum space.

1.3 Reduction to a local problem

Starting from the locality of Σ, the gist of the method consists in mapping the lattice problem into a self-consistent Anderson impurity problem. The relevant equations describing this mapping are formally identical to the ones reported in the literature for the hyper–cubic and the Bethe lattice [7, 8, 9, 10, 16, 49], and we report them here for completeness.

The local Green's function is obtained from the solution of an Anderson impurity problem, whose Dyson equation reads

$$G_{\alpha\sigma}(\omega_n) \;=\; [{\mathcal{G}^{o}_{\alpha\sigma}}^{-1}(\omega_n) \;-\; \Sigma_{\alpha\sigma}(\omega_n)]^{-1}\;, \tag{1.43}$$

where $\Sigma_{i\sigma}[\mathcal{G}^{o}]$ is the local self-energy corresponding to the given $\mathcal{G}^{o}$, $\mathcal{G}^{o}$ being an auxiliary local Green's function which plays the role, formally, of a non-interacting Green's function for the local problem, but actually embodies correlation effects due to the surrounding lattice. The crucial requirement that fixes the choice of $\mathcal{G}^{o}$ is that the resulting $\Sigma_{\alpha\sigma}[\mathcal{G}^{o}]$ and

$G_{\alpha\sigma}$ coincide with the actual self-energy and local Green's function for the lattice problem. This requirement imposes the self-consistency condition

$$G_{\alpha\sigma}(\omega_n) \;=\; \int_0^\infty dE\; \rho(E)\, \frac{Z_\sigma^{\bar\alpha}}{Z_\sigma^A Z_\sigma^B - E^2}\;, \tag{1.44}$$

where

$$Z_\sigma^\alpha \;=\; i\omega_n + \mu + (-1)^R \sigma H_S - \Sigma_{\alpha\sigma}(\omega_n)\;. \tag{1.45}$$

(Here $\bar\alpha$ denotes sublattice B if $\alpha = A$ and viceversa). Eq. (1.44) is nothing but a disguised form of the Dyson equation which relates G and Σ for the lattice problem. A derivation of Eqs. (1.43-1.45) is illustrated in Appendix A. (Notice that in the above equations we have allowed for the presence of a staggered magnetic field H_S which is useful to calculate the staggered susceptibilty of the model). The only difference with the hypercubic case is the non-interacting density of states $\rho(E)$ appearing in Eq. (1.44) which is given in the present case by Eq. (1.20).

Generally speaking, we are interested in two types of solutions of Eqs. (1.43-1.45): (a) A *nonmagnetic* solution in which $G_{\alpha\sigma} \equiv G$ is independent of the sublattice and spin labels; (b) An *antiferromagnetic* solution in which $G_{A\uparrow} = G_{B\downarrow}$ and $G_{A\downarrow} = G_{B\uparrow}$ - a symmetry which has already been used in deriving Eqs. (1.44-1.45) - but $G_{A\uparrow} \neq G_{A\downarrow}$.

The hard part of the task is to solve the local impurity problem, i.e., calculating G (or Σ) for an arbitrary $\mathcal{G}^o$. We have used two very well known approaches: (i) A single-impurity Quantum Monte Carlo simulation using the Hirsch-Fye algorithm at finite temperature [50], which provides in principle an "exact" answer for G [8, 9, 10, 16]; (ii) Alternatively, a very simple perturbative approach - known as Iterated Perturbation Theory (IPT) [9, 10, 16] - which appears to give answers in good agreement with the QMC results, at least within the nonmagnetic phase at half-filling. (See below). It consists in approximating $\Sigma_{\alpha\sigma}[\mathcal{G}^o]$ with the simple second-order diagram, where $\mathcal{G}^o$ is used as a propagator, i.e., (denoting $\bar\sigma = -\sigma$)

$$\Sigma_{\alpha\sigma}(\omega_n) \;=\; U\,\langle n_{\alpha\bar\sigma}\rangle \;+\; U^2\,\frac{1}{\beta}\sum_{\omega_B} \mathcal{G}^o_{\alpha\sigma}(\omega_n - \omega_B)\chi_o^{(\bar\sigma\bar\sigma)}(\omega_B)\;, \tag{1.46}$$

with

$$\chi_o^{(\bar{\sigma}\bar{\sigma})}(\omega_B) \;=\; \frac{1}{\beta}\sum_{\omega_m} \mathcal{G}^o_{\alpha\bar{\sigma}}(\omega_m)\mathcal{G}^o_{\alpha\bar{\sigma}}(\omega_m+\omega_B)\;. \tag{1.47}$$

Here the first term, $U\,\langle n_{\alpha\bar{\sigma}}\rangle$, corresponds to the Hartree diagram and would lead, in absence of any further correction, to the Mean Field approximation. It is crucial that $\mathcal{G}^o$ - and not G or the non-interacting Green's function G^o - is used in these expressions [16]. The agreement with the QMC is quite poor, in fact, if G or G^o are used, except for very small U ($U/t \approx 1$). Nor does it improve by including ladder and ring diagrams in a self-consistent conserving fashion, i.e., with G as a propagator [51]. Fig. 1.5 shows a comparison between the QMC data (solid squares) and the perturbative results obtained using Eq. (1.46) (solid line) for the *nonmagnetic* imaginary time Green's function $G(\tau)$ at $\beta = 8$ ($U/t = 4$ and 8), and for the AF solution $G_{A\uparrow}(\tau)$ in zero external field at $\beta = 6.5$ ($U/t = 4$). The agreement is surprisingly good even for U/t as large as 8 in the nonmagnetic case. It is, however, far less satisfactory if particle-hole symmetry is broken, as when a non-zero magnetization is present - see the inset of Fig. 1.5 - or out of half-filling.

1.4 Numerical results

Single-particle properties are straightforwardly obtained from the Green's function. For instance, the number of particles and the magnetization per site - n and M - are calculated for any given chemical potential μ and staggered field H_S, by using

$$n \;=\; 2 \,+\, \sum_{\sigma} G_{A\sigma}(\tau = 0^+)\;, \tag{1.48}$$

$$M \;=\; G_{A\uparrow}(\tau = 0^+) \,-\, G_{A\downarrow}(\tau = 0^+)\;. \tag{1.49}$$

Fig. 1.6 shows the spontaneous magnetization $M(T)$ in zero field - calculated from IPT - as a function of T for $U/t = 4$. (Solid squares). The Néel temperature is readily obtained by extrapolation of $M(T)$ close to the transition, $T_N/t \approx 0.18$. The critical exponent β is clearly classical, $\beta = 1/2$. The results obtained using the QMC are qualitatively similar - including the value of β - but the actual value of T_N is somewhat larger for this value of U.

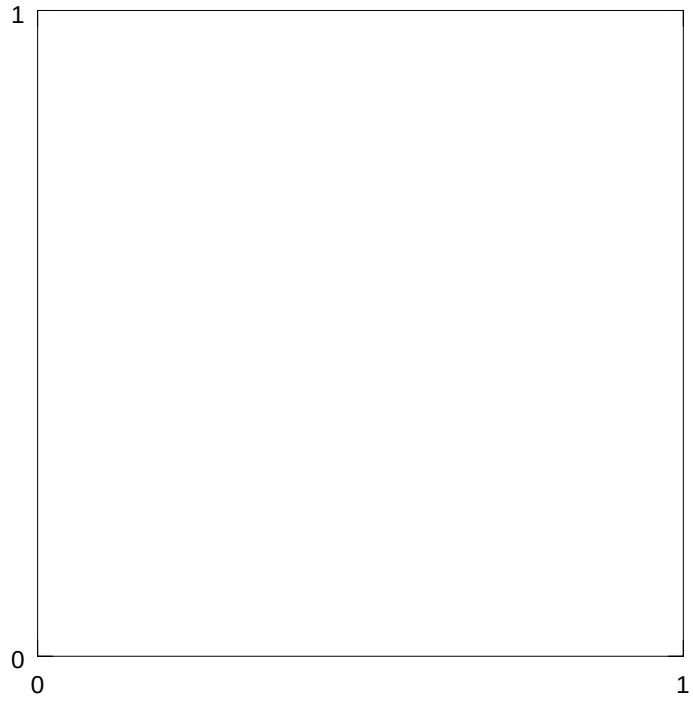

Figure 1.5: Comparison between the QMC (solid squares) and the perturbative (solid lines) results for the nonmagnetic imaginary time local Green's function $G(\tau)$ at $\beta = 8$ ($U/t = 4$ and 8), and (inset) for the AF solution $G_{A\uparrow}(\tau)$ at $\beta = 6.5$ ($U/t = 4$).

This procedure, applied to the QMC data, is used to obtain the Néel transition line shown in the phase-diagram of Fig. 1.9.

Additional information can be obtained from the response functions. Two routes are available for this purpose: (1) We can calculate charge and spin susceptibilities by using the irreducible two-particle vertex parts, obtained from the one-impurity QMC simulation, in the full Bethe-Salpeter equation for the lattice problem, as done in Ref. [8]. (2) If one is interested only in $\mathbf{q} = 0$ properties, for instance in the compressibility $\partial n/\partial \mu$ and the staggered susceptibility $\chi_{sp} = \partial M/\partial H_S$, one has just to take the appropriate *numerical*

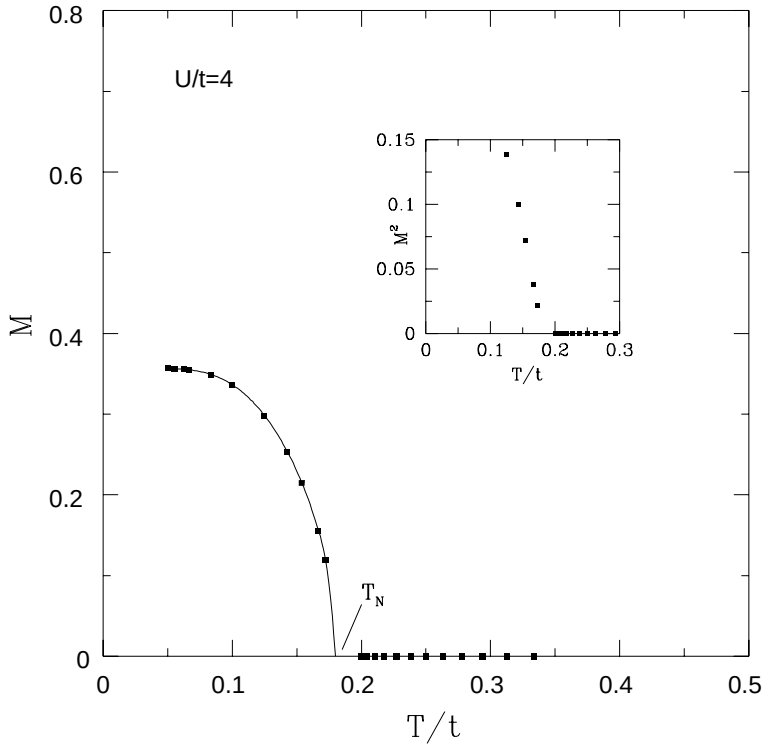

Figure 1.6: The spontaneous magnetization (solid squares) as a function of T for $U/t = 4$. The data shown where obtained using the perturbative approach. The critical exponents coincide with the mean-field Ginzburg-Landau value $\beta = 1/2$.

derivatives of n and M. The latter is, up to now, the only viable method for calculating such quantities within the perturbative approach, for lack of a reliable way of calculating two-particle Green's functions. On the other hand this is not a very practical procedure within the Monte Carlo approach, since the data are plagued by statistical errors, which make the calculation of derivatives quite unreliable. (An exact enumeration algorithm was used for this purpose in Refs. [10, 16]). Fig. 1.7 shows the staggered susceptibility $\chi_{sp}(T)$ - calculated from IPT taking a numerical derivative of M with respect to H_S - as a function of T for $U/t = 4$. (Solid circles). A divergence occurs at T_N, with a critical exponent γ

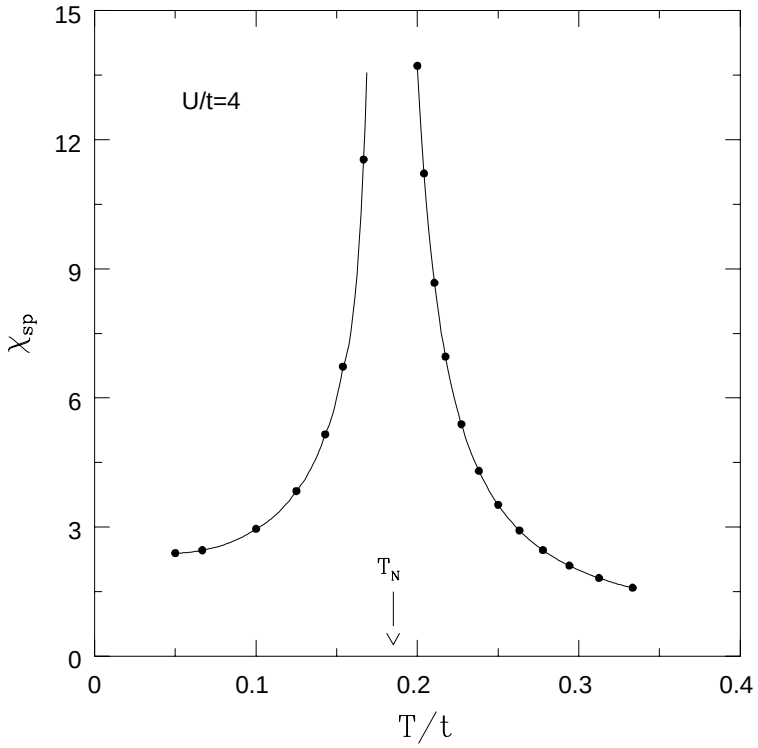

Figure 1.7: The staggered susceptibility as a function of T for $U/t = 4$. The data was obtain using the IPT approach. The critical exponents coincide with the mean-field Ginzburg-Landau value $\gamma = 1$.

for $\chi_{sp}(T)$ which agrees well with the Ginzburg-Landau MF prediction $\gamma = 1$. (Again, qualitatively similar results are obtained using the QMC approach). Fig. 1.8 shows the behavior of the compressibility for $U/t = 4$ and in the same range of temperature of Figs. 1.6 and 1.7. Clearly, the compressibility drops very quickly below the Néel temperature as one would expect if a charge gap has been opened. Indeed, in a single particle picture, a gap Δ results in a compressibility of the form

$$\left.\frac{\partial n}{\partial \mu}\right|_{\text{half-filling}} \approx e^{-\Delta/2k_BT} , \tag{1.50}$$

which well fits our results as shown in the inset of Fig. 1.8. In a semi-metallic phase, on

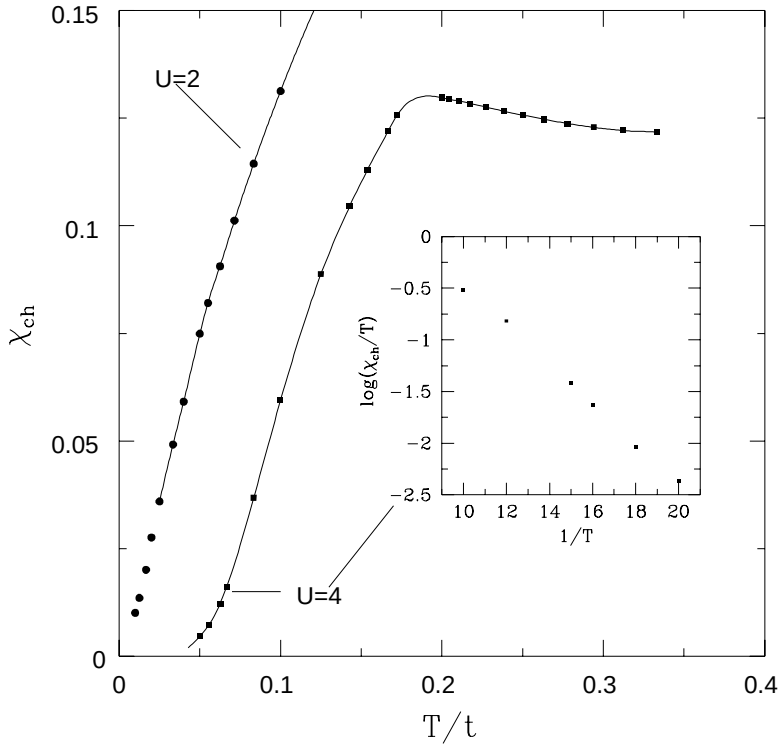

Figure 1.8: Compressibility $\partial n/\partial \mu$ at half-filling versus T for two values of U. For $U/t = 4$ the compressibility shows the presence of a gap in the spectrum, due to the Néel transition just below $T/t = 0.2$, whereas for $U/t = 2$ the typical semi-metallic linear behavior in T is obtained, and there is no AF phase transition.

the contrary, the compressibility is expected to go linearly to zero as $T \to 0$ - $\partial n/\partial \mu \propto T$ - a behavior which is indeed found for $U/t = 2$ and is illustrated by the solid circles in Fig. 1.8. One interesting point to discuss, in this respect, is the possibility of a genuine semi-metal/insulator Mott transition, i.e., one which is *not driven by the onset of the magnetic long range order*. By studying the compressibility $\partial n/\partial \mu$ at half-filling as a function of temperature, we see the opening of a gap below T_N for all the U studied, although it is quite difficult to perform such tests very close to $U_c(T = 0)$. Within our very limited numerical capability for studying fine details, it seems clear that the antiferromagnet is

also an insulator, as perhaps expected from the MF picture.

1.5 Phase diagram

The (U, T) phase-diagram at half-filling, which summarizes our findings - is shown in Fig. 1.9, and compared with that for the hyper-cubic case, shown in the inset. The value of U where the AF phase becomes stable at $T = 0$ is now positive ($U_c/t \approx 2.3$), as expected from HF and from the $D = 2$ results. The non magnetic phase is characterized by a semi-metallic behavior (e.g., a charge compressibility vanishing linearly with T). The remaining features of the phase-diagram have a precise counterpart in the hyper-cubic case, with an overall change of energy scale. In particular, within the non-magnetic (singlet) Hilbert space, the semi-metallic phase would again become unstable (at $T = 0$) against a Mott-Hubbard insulating phase at a critical value of $U_{MH}/t \approx 8.5$. Such a "would be" critical point continues for $T > 0$ as a crossover line schematically sketched by a dashed line in Fig. 1.9, exactly as in the hyper-cubic (or Bethe lattice) case.

As anticipated, the Néel transition line given by IPT is numerically different from the actual QMC result. The solid circles and open squares in Fig. 1.10 show the values of T_N obtained, respectively, from IPT and QMC. (The dashed and solid curves are meant to be a guide for the eye). Clearly, the Néel temperature obtained from IPT is *underestimated* for $U \geq 4$. The reason for such a rather poor performance of IPT with respect to the surprisingly good results for the nonmagnetic $G(\tau)$ shown in Fig. 1.5 is probably due to the fact that IPT loses accuracy as soon as particle-hole symmetry is broken. A particle-hole symmetry breaking is indeed implicit even in the nonmagnetic phase at half-filling if one calculates $\partial n/\partial \mu$ or $\partial M/\partial H_S$ by the numerical derivative method described above: in the first case we have to perform calculations for μ slightly different from the half-filling value of $U/2$, in the second case a small staggered field H_S has to be applied. As soon as particle-hole symmetry is broken the third order (in U) contribution to Σ is no longer

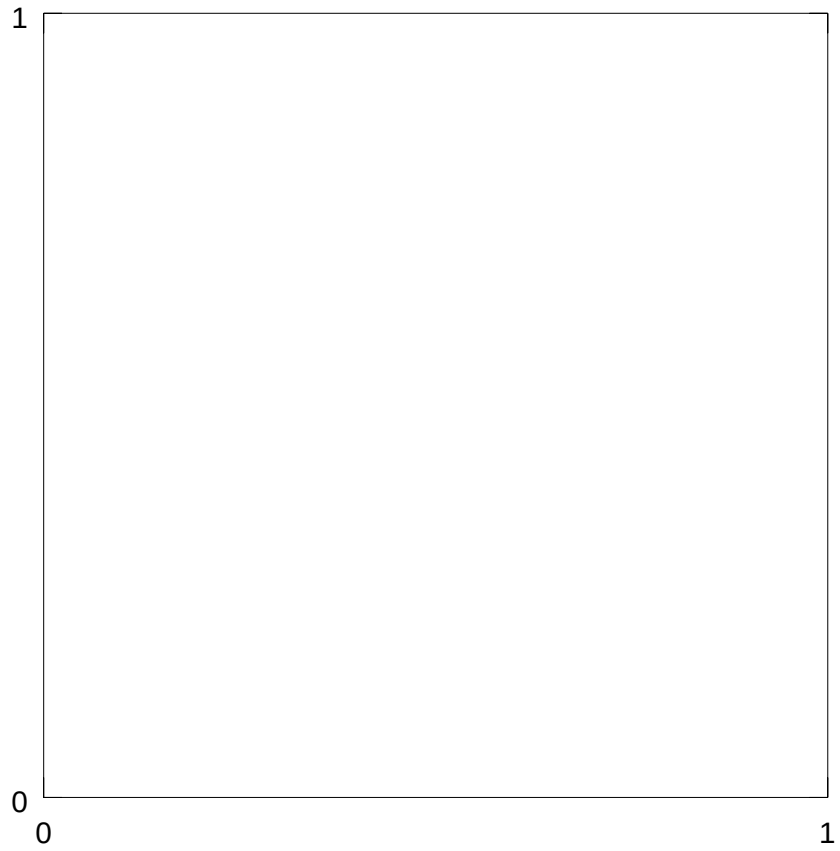

Figure 1.9: (U, T) phase diagram for the Hubbard model on the $D = \infty$ hyper–diamond lattice at half-filling, compared to the hyper-cubic lattice case, schematically sketched in the inset. "NM SM" and "AF INS" stand, respectively, for "nonmagnetic semimetal" and "antiferromagnetic insulator". The critical value of U for the onset of antiferromagnetic long-range order is strictly positive in the hyper-diamond case. U_{MH} indicates the position of the "would be" critical point at which the nonmagnetic semimetal would become unstable to a Mott-Hubbard insulator in absence of AF long-range order.

exactly zero, and - more generally - there is no reason to expect higher orders to be small. (In a way, what is really surprising is that IPT is so good for rather large values of U in the particle-hole symmetric case [52]).

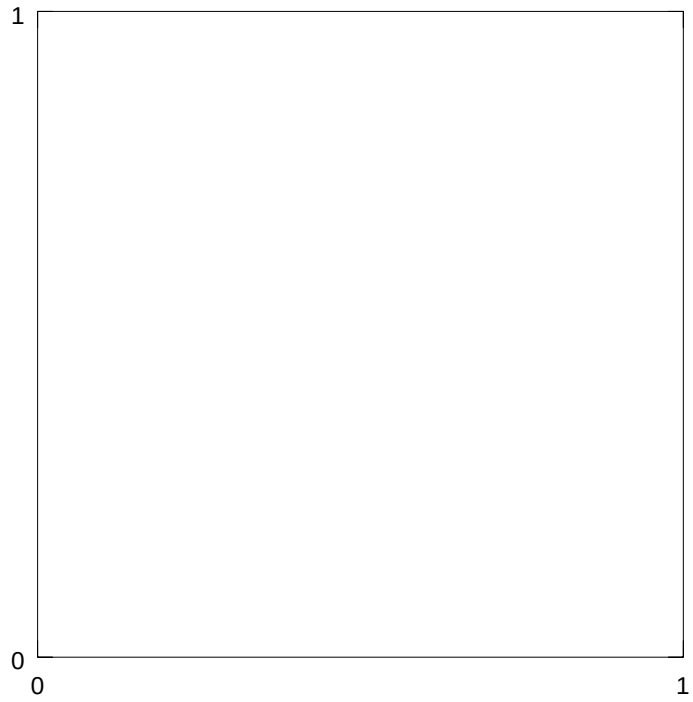

Figure 1.10: Detail of the (U, T) phase diagram for the Hubbard model on the $D = \infty$ hyper-diamond lattice at half-filling, showing the Néel transition line calculated using different methods. The open squares and solid circles represent the results for T_N obtained, respectively, with the QMC and the perturbative approach. (The dashed and solid lines are just guides for the eye). The dot-dashed line shows the mean-field (Stoner) results for T_N.

At $T = 0$ we estimate $U_c/t \approx 2.3$ from QMC and $U_c/t \approx 2.1$ from IPT, whereas a MF theory predicts (at $D = \infty$) a value $U_c^{(MF)}/t = 1.596$. Evidently, quantum fluctuations are not quite as effective as in $D = 2$ in pushing the $U_c(T = 0)$ towards a higher value (in that case $U_c/U_c^{(MF)} \approx 2$, against ≈ 1.5 here), but have not become ineffective either. Moreover,

the disagreement between the MF (Stoner) theory prediction for the Néel temperature $T_N(U)$ (shown in Fig. 1.10 by the dot-dashed curve) and the actual QMC result (solid curve) is more and more pronounced as U increases. In particular, the former has a large–U behavior which is qualitatively wrong - $T_N^{(MF)}(U) \propto U$ - whereas the correct result is expected to be proportional to the strength of the exchange coupling of a spin to the shell of nearest-neighbors, $T_N \sim DJ_D = 4D\tilde{t}^2/U \propto t^2/U$.

Finally, a few comments on the much debated issue [9, 10, 16] of a Mott transition not driven by AF long-range order are appropriate. If we ignore the possibility of the onset of AF long range order by *not looking at the corresponding response function* (i.e. the staggered susceptibility, which happens to diverge below some T_N, for U above some U_c), we keep finding a nonmagnetic solution of our self-consistent equations (1.43)-(1.44) for the Green's function which appear to be perfectly legitimate. The $U/t = 8$ result in Fig. 1.5 illustrates such an occurrence. The one-particle Green's function is totally blind, in this respect, to the magnetic transition. By insisting on a nonmagnetic solution, the system would sooner or later open up a gap, upon increase of U, by breaking the Fermi liquid: this is the Mott transition dealt with in Refs. [9, 10, 16]. For the model we are considering, we find that this happens (at $T = 0$) for $U_c/t \approx 8.5$. It is worth stressing, however, that for all the nearest-neighbor hopping bipartite lattices considered so far, such a nonmagnetic solution is strictly *unstable* (at $T = 0$) in the region where the Mott transition would occur. The genuine $T = 0$ "Mott transition" is preempted by the magnetic instability, and its actual relevance seems therefore confined, so far, to models where disorder inhibits AF long-range order [17].

2 Correlated Electrons in a Lattice of Jahn–Teller Molecules.

In this Chapter we study a lattice of molecules described by an E–e type of Jahn–Teller hamiltonian both in the weak and in the strong electron-phonon coupling regime.
The Chapter is organized as follows: In Section 2.1 we introduce the model and discuss the properties of a single molecule. Section 2.2 is devoted to the derivation of an effective electronic hamiltonian for a lattice of such Jahn–Teller molecules both in the weak and in the strong coupling limit. In Section 2.3 we show that the solution for two electrons can be carried out exactly and the corresponding two–particle ground state can be represented as a dimer state. This interpretation leads, in both limits, to a common physical picture of the system at low density as a dilute gas of these pre–existing dimers. In Section 2.4, we analyze the weak electron–phonon coupling limit of the model within a BCS mean field approach. Finally, in Section 2.5, we study the model in the strong on–site repulsion regime.

2.1 The molecule

The model we are going to discuss describes an array of molecules with two degenerate electronic orbitals $c_{1\sigma}$ and $c_{2\sigma}$ (later referred to as "bands"), coupled to a two-dimensional molecular vibration (henceforth called phonon) with energy ω_0 ($\hbar = 1$). Each molecule is

described by the so called E–e hamiltonian:

$$H_{mol} = \frac{\omega_0}{2}\left(\vec{r}^{\,2} + \vec{p}^{\,2}\right) + g\omega_0 \vec{r}\cdot\vec{\tau}\,, \tag{2.1}$$

where $\vec{r} = (x, y)$ is the two-dimensional coordinate of the local phonon mode, and

$$\vec{\tau} = \frac{1}{2}\sum_{a,b=1,2}\sum_{\alpha=\uparrow,\downarrow} c^{\dagger}_{a\alpha}\vec{\sigma}_{ab}c_{b\alpha}\,, \tag{2.2}$$

being $\vec{\sigma}$ the Pauli matrices.

By introducing the two annihilation (and creation) operators associated to the phonon modes:

$$a_{1(2)} = \frac{1}{2}\left[(x \pm iy) - i\,(p_x \pm ip_y)\right]\,, \tag{2.3}$$

the E–e Jahn–Teller hamiltonian, defined in Eq. (2.1), can be rewritten, in a more suitable way, as:

$$H_{mol} = \omega_0\left(a_1^{\dagger}a_1 + a_2^{\dagger}a_2\right) + g\frac{\omega_0}{2}\left[\tau^{+}\left(a_1 + a_2^{\dagger}\right) + \tau^{-}\left(a_2 + a_1^{\dagger}\right)\right]\,, \tag{2.4}$$

where $\tau^{+} = \tau_x + i\tau_y$ and $\tau^{-} = \tau_x - i\tau_y$.

The hamiltonian (2.1) has to be compared with that describing single–band electrons coupled to a non–degenerate phonon

$$H_{mol} = \frac{\omega_0}{2}\left(r^2 + p^2\right) + g\,\omega_0\, r\, n\,, \tag{2.5}$$

where r is the one-component phonon coordinate and

$$n = \sum_{\alpha=\uparrow,\downarrow} c^{\dagger}_{\alpha}c_{\alpha}$$

is the local density of single band electrons. In what follows we will show that the additional degrees of freedom of (2.1) give rise to new interesting properties.

In the absence of electron-phonon coupling, each molecular level of the Hamiltonian (2.1) with vibronic energy $m\omega_0$ and n electrons is degenerate, with degeneracy

$$(m+1)\times\begin{pmatrix} 4 \\ n \end{pmatrix}.$$

The binomial coefficient counts the number of ways of distributing n fermions among 4 levels (1 and 2, $\uparrow$ and $\downarrow$). These states can be labeled for instance by the total spin S, its z-component S_z, and by τ_z (which is half the difference between the number of electrons in orbital 1 and that one in orbital 2). The factor (m+1) is instead the degeneracy of each vibrational state and corresponds to the possible values that the vibron angular momentum $L_z = xp_y - yp_x$ can assume ($L_z = -m, -m+2, ..., m$). When the electron-phonon coupling is switched on, this degeneracy is lifted. The total spin and its z-component are still good quantum numbers, but now only the z-component of the total pseudo angular momentum

$$J_z = L_z + \tau_z,$$

commutes with the Hamiltonian [18]. Notice that for odd number of electrons τ_z is half–integer and, consequently, so is J_z. Due to the symmetry $J_z \to -J_z$, each state (also the ground state) with odd number of electrons is at least four-fold degenerate ($\pm J_z$, $S = \pm 1/2$). On the contrary for even number of electrons the starting degeneracy is split and the ground state turns out to be an orbital, as well as a spin, singlet.

At weak electron-phonon coupling $g \ll 1$ each multiplet is split by energy shifts of order $\omega_0 g^2$, but different multiplets are still well separated by energy ω_0. If we are interested in the behavior of the model at energies $\ll \omega_0$, we can neglect all but the lowest multiplet. Since this is adiabatically connected to the multiplet without excited vibrons ($m = 0$, $L_z = 0$), it can be labelled by the electronic quantum numbers only (S, S_z and τ_z). This suggests that it is possible to define an effective Hamiltonian for this lowest multiplet which acts only on the electronic degrees of freedom and is able to reproduce the energy shifts inside the multiplet. This is just what we are going to do.

A standard way to derive this Hamiltonian is via an ordinary perturbation theory in the small parameter g, which is best done using the alternative formulation (2.4). Neglecting retardation effects, which means that the lattice deformations has to follow instantaneously the electrons, the electron–phonon coupling leads to an indirect interaction between elec-

trons. The effective hamiltonian reads:

$$H_{MOL} = -\omega_0 \frac{1}{2} g^2 (1 - \frac{g^2}{2}) \vec{\tau}^2 - \omega_0 \frac{3}{8} g^4 \tau_z^2 \,, \tag{2.6}$$

which is expected to give the correct answer up to order g^4.

It easy to verify that the molecular ground state with an odd number of electrons ($n = 1, 3$) is four–fold degenerate ($J_z = \pm 1/2, S_z = \pm 1/2$), and its ground state energy is, up to order g^4, $E_{n=1,3}/\omega_0 = -g^2/4 + g^4/32$. On the other hand, for two electrons, the electron-phonon interaction splits the initial six–fold degenerate ground state state into a multiplet whose lowest member is a non–degenerate singlet ground state ($J_z = 0, S = 0$). More precisely (in units of ω_0):

$$\begin{aligned} E_2(J_z = 0, S = 0) &= -g^2 + g^4/2 \,, \\ E_2(J_z = \pm 1, S = 0) &= -g^2/2 - g^4/8 \,, \\ E_2(J_z = 0, S = 1) &= 0 \,. \end{aligned} \tag{2.7}$$

The same results can be also obtain by means of an unitary transformation [25]. For a comprehensive review on unitary transformations in Jahn–Teller models see, for instance, Wagner in Ref. [53].

In the strong coupling limit $g \gg 1$, the situation is quite different. The ground state has the same quantum numbers as in the weak coupling limit, i.e. $S = 1/2$ and $J_z = \pm 1/2$ for odd numbers of electrons, and $S = 0$ and $J_z = 0$ for even numbers. The lowest excited states have now the same spin but higher J_z (apart from the trivial case of 0 and 4 electrons, where there is no Jahn-Teller distortion), and they are separated from the ground state by an energy of the order $\omega_0 J_z^2/g^2$.

2.2 Lattice of molecules

Let us consider a lattice of E-e molecules coupled by the single particle hopping term:

$$H_{HOP} = -t \sum_{<r,r'>} \sum_{\sigma} \left[c^{\dagger}_{1,r,\sigma} c_{1,r',\sigma} + c^{\dagger}_{2,r,\sigma} c_{2,r',\sigma} \right]. \tag{2.8}$$

Electron hopping between two neighboring molecules modifies both their spin S and their pseudo angular momentum J_z. Therefore it will mix the ground state configurations of each molecule with the excited states of the others. In the two following subsections we discuss this problem both in the weak and in the strong electron–phonon coupling limit.

2.2.1 Weak coupling limit

In the weak coupling limit $g \ll 1$, if moreover $t\,g \ll \omega_0$, we can retain just the hopping processes which mix the states in the lowest multiplet for each electron occupancy. By means of a perturbation theory in g, we find:

$$\begin{aligned} H_{HOP} \;=\; & -t' \sum_{<r,r'>} \sum_{\sigma} \Big[c^{\dagger}_{1,r,\sigma} c_{1,r',\sigma} + \frac{g^4}{8} c^{\dagger}_{1,r,\sigma} c_{1,r',\sigma} \left(n_{2,r,-\sigma} + n_{2,r',-\sigma} - n_{1,r,-\sigma} - n_{1,r',-\sigma} \right) \\ & - \frac{g^4}{8} c^{\dagger}_{1,r,\sigma} c_{1,r',-\sigma} \left(c^{\dagger}_{2,r,-\sigma} c_{2,r,\sigma} + c^{\dagger}_{2,r',-\sigma} c_{2,r',\sigma} \right) + (1 \leftrightarrow 2) \Big] + H_3 \,, \end{aligned} \tag{2.9}$$

where $t' = t\,(1 - g^2/8 + 3g^4/64)$ is the effective hopping, and H_3 is a three–body hopping term which is different from zero only when one of the two sites involved in the hopping process is occupied by three electrons (in the initial or in the final state):

$$\begin{aligned} H_3 \;=\; & -t' \frac{g^4}{4} \sum_{<r,r'>} \sum_{\sigma} c^{\dagger}_{1,r,\sigma} c_{1,r',\sigma} \left[n_{2,r',\sigma} \left(n_{1,r'-\sigma} - n_{2,r'-\sigma} \right) + n_{2,r,\sigma} \left(n_{1,r-\sigma} - n_{2,r-\sigma} \right) \right] \\ & + \; c^{\dagger}_{1,r,\sigma} c_{1,r',-\sigma} \left[n_{1,r',\sigma} c^{\dagger}_{2,r',-\sigma} c_{2,r',\sigma} + n_{1,r,-\sigma} c^{\dagger}_{2,r,-\sigma} c_{2,r,\sigma} \right] + (1 \leftrightarrow 2) \,. \end{aligned} \tag{2.10}$$

The H_3 term is important in order to preserve the invariance of the model under a particle–hole transformation ($c_{a,r,\sigma} \rightarrow (-1)^r c^{\dagger}_{a,r,\sigma}$, $a = 1,2$). However, if we suppose that the Coulomb repulsion is sufficiently strong, the large on–site occupancies (three or four electrons per site) are forbidden and the H_3 term can be dropped. Therefore, in the following,

we will always forget this term.

From Eq.(2.9) we see that the electron–phonon interaction modifies the hopping amplitude according to the occupation of the sites involved in the hopping process. In particular, if we restrict to the lowest–energy molecular states, the hopping amplitude from (or into) a doubly occupied site ($J_z = S = 0$) increases relatively to the hopping from a single occupied site (also in the molecular ground state) to an empty one. For instance the hopping process from a doubly occupied site to a nearest neighboring empty site, relative to that from a singly occupied site to an empty site is $T_{2\to 0}/T_{1\to 0} = (1 + g^4/4)/\sqrt{2}$ for small g (while $T_{2\to 0}/T_{1\to 0} \to 1$ at large g [23]).

To summarize, for sufficiently small electron-phonon coupling g, the effective hopping hamiltonian (2.9) plus the molecular term (2.6) describes a lattice of E–e molecules even in the interesting weakly anti-adiabatic limit $t \sim \omega_0$. In order to describe a more realistic system, we also include a generalized on–site interaction including Hund's rule exchange in the form:

$$\begin{aligned} H_{ON-SITE} &= U_1 \sum_{r,\sigma,\sigma'} n_{1,r,\sigma}\, n_{2,r,\sigma'} - U_2 \sum_r \vec{S}_{1,r} \cdot \vec{S}_{2,r} \\ &\quad + \frac{U_3}{2} \sum_{r,\sigma} \left(n_{1,r,\sigma} n_{1,r,-\sigma} + n_{2,r,\sigma} n_{2,r,-\sigma} \right) , \end{aligned} \tag{2.11}$$

where $\vec{S}_a$ is the spin operator of electrons $a = 1, 2$. U_1, U_2 and U_3 is in fact the minimal set of parameters, describing the two–particle six–state three–level multiplet.

In conclusion the total effective hamiltonian reads:

$$H_{TOT} = H_{HOP} + H_{ON-SITE} + \sum_r H_{MOL}(r) . \tag{2.12}$$

2.2.2 Strong coupling limit

At strong coupling the situation is more complicated. In fact the number of lowest excited states, characterized by higher J_z, with excitation energy $\leq \omega_0$, grows like g for large g, and therefore greatly exceed the analogous number in the weak coupling limit (which coincides with the number of states in the lowest multiplet, i.e. six for two electrons). In order to simplify the analysis the excitations into these higher-J_z states can be forbidden [23, 24].

This amounts to assume that the matrix elements due to the hopping processes which mix these states with the molecular ground state configurations, are much smaller than the excitation energies, that is

$$t \ll \frac{\omega_0}{g^2} .$$

In such limit of validity Ref.[23] introduced an effective hamiltonian with a single electronic level which guarantees that the doubly occupied site is always in a singlet state. The larger occupancies were disregarded by imagining a strong on–site repulsion able to cancel the strong polaronic binding energy (of order $\omega_0 g^2$). The role of the quantum number J_z was mimicked by an extra spin–1 degree of freedom associated to each site of the lattice: the allowed spin–1 states at each site depend on the electron occupancy. More precisely, an empty or doubly occupied site must have $S^z = 0$ (which corresponds to $J_z = 0$), whereas a site occupied by a single electron (either up or down) has an additional two–fold (orbital) degeneracy, represented by $S^z = \pm 1$ (which corresponds to $J_z = \pm 1/2$),

$$\begin{aligned} n_r = 0, 2 \quad &\longrightarrow \quad S^z_r = 0 \ , \\ n_r = 1 \quad &\longrightarrow \quad S^z_r = \pm 1 \ . \end{aligned} \tag{2.13}$$

The effective hamiltonian $H_{g=\infty}$ is written as follows:

$$H_{g=\infty} \ = \ -\frac{t'}{2} \sum_{<r,r'>} \sum_{\sigma} \left(c^{\dagger}_{r,\sigma} c_{r',\sigma} + h.c.\right) \left(S^{+}_{r} S^{-}_{r'} + h.c.\right) + \left(U - \frac{3}{4}\omega_0 g^2\right) \sum_{r} n_{r,\uparrow} n_{r,\downarrow} \ , \tag{2.14}$$

where t' is the effective hopping (the original hopping t reduced by the Ham factor), the $S^{\pm}_r$'s are spin–1 ladder operators at each site, and the remaining notation is completely standard. We have also included in the hamiltonian (2.14) an on–site Hubbard repulsion U, which is able, in principle, to overcome the polaronic contribution $-3/4\,\omega_0 g^2$.
It is worth stressing that while $H_{g=\infty}$, and in particular the hopping term, *conserves the constraint* in Eq. (2.13), the model is still highly non-trivial.

In one dimension the effective hamiltonian (2.14) can be represented in a more suitable form, which involves only fermionic operators, without resorting to the introduction of an extra spin–1. This can be done by introducing two additional hard–core boson operators

$d_\uparrow$ and $d_\downarrow$ at each site of the lattice. Next, on each singly-occupied site we identify $S^z = 1$ ($S^z = -1$) with the presence of the boson $d_\uparrow$ ($d_\downarrow$ respectively). On the other hand, doubly occupied sites ($S^z = 0$) are represented with two bosons $d_\uparrow d_\downarrow$, while empty sites ($S^z = 0$) are characterized by no bosons at all. Using this mapping the constraint (2.13) assumes the more convenient form:

$$\sum_\sigma n^d_{r,\sigma} \;=\; \sum_\sigma n^c_{r,\sigma} \;, \tag{2.15}$$

where $n^c_{r,\sigma} = c^\dagger_{r,\sigma} c_{r,\sigma}$ and $n^d_{r,\sigma} = d^\dagger_{r,\sigma} d_{r,\sigma}$. The effective hamiltonian (2.14) can be rewritten, in this case, as:

$$\begin{aligned} H_{g=\infty} \;&=\; -t' \sum_{<r,r'>} \sum_{\sigma,\sigma'} \{\, c^\dagger_{r,\sigma} c_{r',\sigma} d^\dagger_{r,\sigma'} d_{r',\sigma'} + h.c. \,\} \\ &+\; \frac{U - \frac{3}{4}\,\omega_0\, g^2}{2} \sum_r [\, n^c_{r,\uparrow} n^c_{r,\downarrow} \;+\; n^d_{r,\uparrow} n^d_{r,\downarrow} \,] \;. \end{aligned} \tag{2.16}$$

Up to this point the mapping is valid in any dimensions. In the 1D case, a Jordan–Wigner transformation, allows to transform the hard–core bosons $d_{r,\sigma}$ into fermion operators. In such a case the resulting effective hamiltonian $H_{g=\infty}$ assumes a more symmetric form and the $SU(2) \times SU(2)$ symmetry of the model becomes manifest.

The main difficulty with these representations ((2.14) and (2.16)) is to implement the condition that J_z is half an odd integer for a singly occupied site and integer otherwise; one had to impose the constraint (2.13) (or the equivalent one given in Eq. (2.15)) which, as usual in quantum mechanics, is very hard to deal with.

In the weak electron–phonon coupling limit ($g \to 0$), by working in the lowest multiplet for each occupancy, the above condition is automatically satisfied. Therefore one does not need such a constraint, which permits to perform a more systematic analysis of the model by analytical techniques without resorting to numerical methods.

2.3 The two–particle solution and the low–density limit

The two–particle problem can be solved exactly both in the weak and in the strong electron–phonon coupling regime.

2.3.1 Strong coupling limit, $g \to \infty$

A generic state in the two-particle Hilbert space with total z-component of the spin $M^z_{TOT} = 0$ (for both the electron spin and the spin–1 states) can be written as:

$$|\Psi\rangle = \sum_{r,r'} \left[\psi_{+-}(r,r')\, S^+_r S^-_{r'} + \psi_{-+}(r,r')\, S^-_r S^+_{r'} \right] c^\dagger_{r,\uparrow} c^\dagger_{r',\downarrow} |0\rangle \,, \tag{2.17}$$

where the vacuum $|0\rangle$ is the state without fermions and with $S^z_r = 0$ at each site. In writing $|\Psi\rangle$ we have taken into account the two possibilities of associating a $S^z = \pm 1$ spin state to the up and down electrons: ψ_{+-} is the amplitude for having $S^z = +1$ associated to the $\uparrow$-electron (and $S^z = -1$ to the $\downarrow$-electron), while ψ_{-+} is the amplitude for other possible choice. The Schrödinger equation for $\psi_{+-}(r,r')$ is easily shown to be

$$\begin{aligned} E\psi_{+-}(r,r') \;=\; & -t' \sum_{\mathbf{a}} \left[\psi_{+-}(r+\mathbf{a},r') + \psi_{+-}(r,r'+\mathbf{a}) \right] + (U - \frac{3}{4}\omega_0 g^2)\, \delta_{r,r'}\, \psi_{+-}(r,r') \\ & -t' \Big(\sum_{\mathbf{a}} \delta_{r+\mathbf{a},r'}\Big) \left[\psi_{-+}(r,r) + \psi_{-+}(r',r') \right] , \end{aligned} \tag{2.18}$$

where $\mathbf{a}$ denotes a nearest neighbor vector ($\mathbf{a} = \pm 1$ in 1D). A similar equation is obtained for $\psi_{-+}(r,r')$ by just exchanging ψ_{-+} and ψ_{+-} everywhere. The last term in Eq. (2.18) is crucial to the whole story, and deserves a few comments. When the two electrons are far enough in the otherwise empty lattice, the hamiltonian $H_{g=\infty}$ simply allows the hopping to a nearest neighbor site of the "composite" object formed by an electron and the associated spin–1 state (first term in Eq. (2.18)). Things are more subtle when two electrons come to the same site r. In such a case, from a doubly occupied site with $S^z_r = 0$ one can reach, upon hopping, two possible final states: either each electron keeps its own spin–1 state or the spin–1 states associated to the two electrons are exchanged. It is precisely this second

possibility of exchanging spin–1 states that is responsible for the presence of $\psi_{\mp}$ in the equation for $\psi_{\pm}$ and vice-versa (last term in Eq. (2.18)).

The Schrödinger equation (2.18) is easily solved in momentum space, where it reduces to a 2×2 matrix problem. The set of solutions, among which the ground state is found, satisfies the equation

$$\frac{1}{L^D} \sum_k \frac{1}{E - \epsilon_k - \epsilon_{P-k}} = \frac{2}{E + U - \frac{3}{4}\omega_0 g^2} \,, \tag{2.19}$$

where E is the energy eigenvalue, P is the total momentum and ϵ_k is the tight-binding dispersion of the free-electron problem ($\epsilon_k = -2t' \sum_{j=1}^{D} \cos k_j$).

2.3.2 Weak coupling limit, $g \to 0$

Now we are going to solve the two–particle problem in the weak electron–phonon coupling regime.

In close analogy to the previous case, a generic state for two particles, with total $J_z = 0$, has the form:

$$|\Psi\rangle = \sum_{r,r'} \left[\psi_{\pm}(r,r')\, c^{\dagger}_{1,r,\uparrow} c^{\dagger}_{2,r',\downarrow} + \psi_{\mp}(r,r')\, c^{\dagger}_{2,r,\uparrow} c^{\dagger}_{1,r',\downarrow} \right] |0\rangle \,, \tag{2.20}$$

where $|0\rangle$ is the state without electrons.

Also in this case the two–particle problem is easily solved in the momentum space. The eigenvalue equation for the energy E reads:

$$\frac{1}{L^D} \sum_k \frac{1}{E - \epsilon_k - \epsilon_{P-k}} = \frac{1 + \frac{1}{2}g^4}{\frac{1}{2}Eg^4 + U_1 + \frac{3}{4}U_2 - \frac{1}{2}\omega_0 g^2 + \frac{7}{16}\omega_0 g^4} \,. \tag{2.21}$$

2.3.3 Two–particle bound state and the low–density limit

Both equations (2.19) and (2.21) can be rewritten in the unique following form:

$$\frac{1}{L^D} \sum_k \frac{1}{E - \epsilon_k - \epsilon_{P-k}} = \frac{2r(g)^2}{E\,[2r(g)^2 - 1] + U_S} \,, \tag{2.22}$$

where $r(g)$, the ratio between the hopping from a doubly occupied site ($J_z = S = 0$) to an empty site and the hopping from a singly occupied site to an empty one, is given by:

$$r(g) = \begin{cases} \frac{1}{\sqrt{2}}\left(1 + \frac{g^4}{4}\right) , & g \to 0 , \\ 1 , & g \to \infty , \end{cases}$$

and U_S is the on–site repulsion relatively to a singlet state:

$$U_S = \begin{cases} U_1 + \frac{3}{4}U_2 - \frac{1}{2}\omega_0 g^2 + \frac{7}{16}\omega_0 g^4 , & g \to 0 , \\ U - \frac{3}{4}\omega_0 g^2 , & g \to \infty . \end{cases}$$

In the ordinary Hubbard case, the right hand side of Eq. (2.22) would simply read $1/U$ [54]. A simple analysis shows that equation (2.22) admits a bound state solution, both in one and two dimensions, as soon as $r(g) > 1/\sqrt{2}$, i.e. for $g > 0$, even in presence of a repulsive on–site interaction U_S, up to:

$$U_S^c = 4D \left[2\, r(g)^2 - 1 \right] t' , \tag{2.23}$$

where D is the space dimensionality. Notice that this bound state, for $0 < U_S < U_S^c$, is a peculiar feature of the degenerate model and it is absent for the non–degenerate version (2.5). Remarkably, the attraction responsible for this binding is *generated by a kinetic process* via the presence of additional degrees of freedom. On the other hand, in $D \geq 3$ a finite attractive U_S is needed to produce a bound state.

The bound state solution can be worked out analytically in 1D. For general values of the total momentum P and for $U_S \leq U_S^c$, the ground state energy is given by

$$E_P = \frac{U_S \left[2r(g)^2 - 1\right] - 2r(g)^2 \sqrt{U_S^2 + 8\,(1 + \cos P)\, t'^2 \left[4r(g)^2 - 1\right]}}{4r(g)^2 - 1} \tag{2.24}$$

and the corresponding ground state wave-function, for $P = 0$, is:

$$\psi_\pm = \psi_\mp \propto \left[e^{-\lambda |r - r'|} - \text{const.}\, \delta_{r,r'} \right] , \tag{2.25}$$

with

$$\lambda = -\log \frac{U_S + \sqrt{U_S^2 + 16\, t'^2 \left[4r(g)^2 - 1\right]}}{4\, t' \left[4r(g)^2 - 1\right]} . \tag{2.26}$$

At larger values of U_S, no bound state is present and the energy spectrum is continuous in the infinite lattice. The two–particle solution cannot be generalized to an arbitrary number of particles by Bethe Ansatz because the corresponding scattering matrix does not satisfy the Yang–Baxter relations.

The wavefunction Eq. (2.25) naturally provides a picture of bound pairs approximately localized on adjacent lattice sites, thereby forming *dimers*. This is a consequence of the kinetic origin of the paring mechanism which delocalizes the pair on neighboring sites. The same feature is also present in two dimensions where a even more efficient delocalization of the electron pair, due to the larger coordination of the 2D lattice, allows a larger value of the critical on–site repulsion U_S^c.

This interpretation of the two–particle ground state in terms of a dimer state leads to a simple picture, at least for $U_S < U_S^c$, of the low density limit of the system, both in one and two dimensions: The system behaves as a weakly interacting, dilute gas of dimers. These dimers follow boson statistics and may be thought of as bosons with an extended core. In order to characterize these composite particles, we can estimate their effective mass from our two–particle calculation. In fact, Eq. (2.24) can be interpreted as the "single dimer dispersion relation" which, at small momentum P gives $E_P \sim E_0 + t_{\rm eff}(g)P^2$ with

$$t_{\rm eff}(g) = t' \frac{r(g)^2}{\sqrt{(\frac{U_S}{4t'})^2 + 4r(g)^2 - 1}} \,. \tag{2.27}$$

The effective mass has a smooth dependence on U_S varying between $\frac{\sqrt{4r(g)^2-1}}{r(g)^2}$ at $U_S = 0$ and 2 at $U_S = U_S^c$. Dilute dimers seem therefore rather mobile and then a superfluid ground state must be expected at zero temperature. In one dimension, of course, off–diagonal long range order cannot occur and only a long range power law decay of the dimer density matrix is possible, while in two dimensions a genuine Bose condensate will form. In terms of the original electrons this implies a standard strong coupling BCS superconducting ground state with localized Cooper pairs. A similar scenario has also been proposed in the framework of the one dimensional $t - J$ model where bound pairs are formed at low density [30] and

$2 < J/t < 2.95$. In that case, however, the model is unstable to phase separation, which in fact occurs massively at larger values of J/t.

In order to check whether the superfluid dimer picture is correct and if our model is free of such an instability at low density, we have carried out a numerical investigation of the four–particle problem, at $U_S = 0$ and $g \to \infty$, by exact diagonalization of $H_{g=\infty}$ (Eq. (2.14)) in lattices up to 24 sites. The results for the ground state energy and for the density–density correlation function are reported in Figs. 2.1 and 2.2.

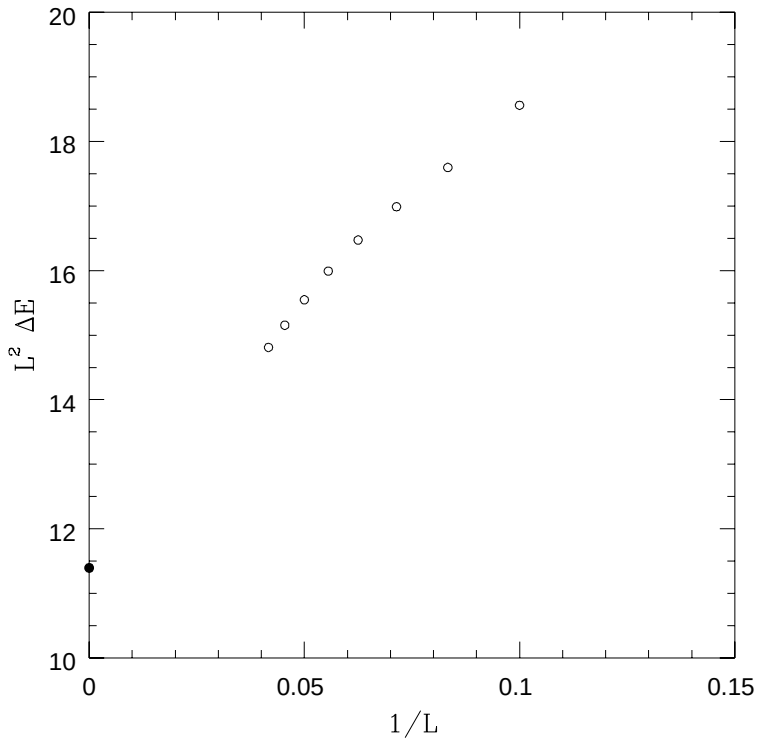

Figure 2.1: Size scaling of the ground state energy of the hamiltonian in Eq. (2.14) with $U_S = 0$ and four electrons. $\Delta E = E_L(4) - 2E_\infty(2)$ where $E_L(N)$ is the ground state energy of N electrons in a L-site ring in units of t'. The full circle is the exact result for two hard-core bosons in the infinite lattice with $t_{\rm eff}(g = \infty) = t'/\sqrt{3}$.

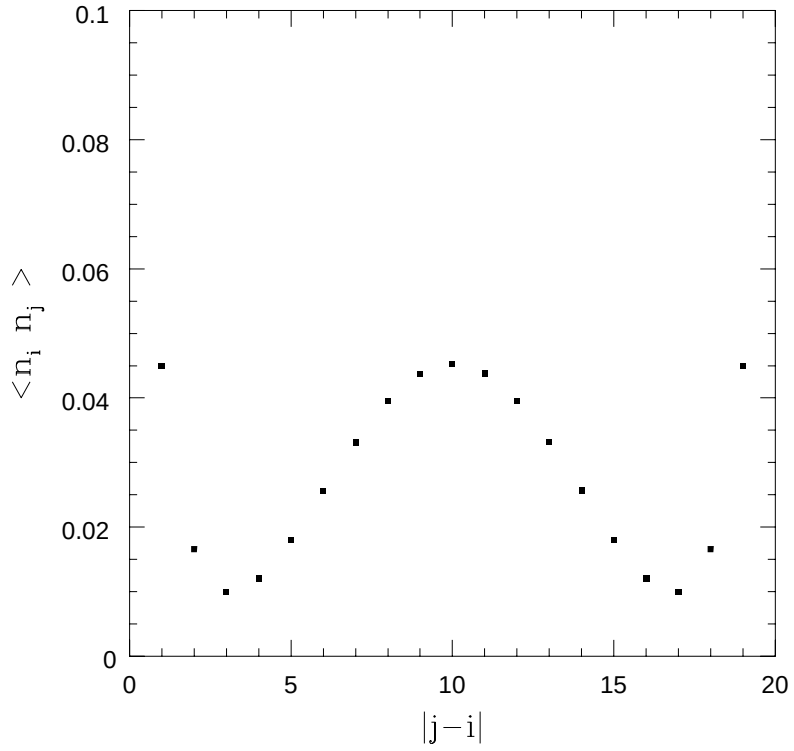

Figure 2.2: Plot of the density-density correlation function for four electrons in a $L = 20$-site ring at $U_S = 0$ and $g \to \infty$.

The finite size scaling of the energy of four electrons clearly shows that the limiting value is just twice the pair energy $E_P(g = \infty) = -8\,t'/\sqrt{3}$ with $1/L^2$ corrections, as expected from the free "hard core boson" representation of the dimers. The same picture is confirmed by the repulsive nature of the pair correlation function: The four electrons are sharply localized in two pairs placed at the maximum separation (antiperiodic boundary conditions are imposed in our computation). The origin of this repulsion is purely kinetic and is also reproduced by the ground state wavefunction of two hard core bosons in one dimension $\psi(R) \propto |\sin(\pi R/L)|$. This suggests that the leading size dependence of the ground state energy is given by the hard core boson result with the appropriate effective

dispersion $t_{\rm eff}(g=\infty) = t'\left[3+(U/4t)^2\right]^{-1/2}$. This scenario would give the asymptotic result $L^2(E-2\,E_0) \to 2\pi^2\, t_{\rm eff}(g=\infty)$ marked with a full circle in Fig. 2.1. The numerical results for finite chains are clearly compatible with this estimate, suggesting that the hard core boson picture holds at low density and $U_S < U_S^c$.

2.4 BCS-Mean Field Solution in the weak electron–phonon coupling regime

In the previous section we have discussed the physics of the low density limit in one and two dimensions. Here the situation is rather clear. A phase transition occurs at $U_S = U_S^c$ between a superconductor and a normal metal.
A natural question is whether and how this transition survives also at finite density. A BCS mean field theory can be very useful in order to clarify this aspect of the problem. However, in the strong electron–phonon regime, the constraint (2.13) makes the BCS approach hard to treat. On the opposite hand, for $g \to 0$, the constraint is not present at all. In such a situation the BCS theory can be implemented in a successful way.

In this section we study the instability to superconductivity of our model, in the weak electron–phonon coupling limit, within the BCS mean field theory and we provide an analytical determination of the phase boundary between the superconducting and the normal state.

In Sections 2.2 we have shown how the lattice of E-e molecules can be mapped in the weak coupling limit ($g \ll 1$ and $tg \ll \omega_0$) onto the model with the Hamiltonian (2.12) where only electronic degrees of freedom appear.

The BCS wave function we use to minimize the energy of hamiltonian (2.12) is

$$|\Phi_0\rangle = \prod_k \left[u_k + \frac{v_k}{\sqrt{2}} \left(c^\dagger_{1k\uparrow} c^\dagger_{2-k\downarrow} + c^\dagger_{2-k\uparrow} c^\dagger_{1k\downarrow} \right) \right] |0\rangle \,.$$

The interaction between the Cooper pairs is given by:

$$V_{\mathbf{k}\mathbf{k}'} = U_1 + \frac{3}{4}U_2 - \frac{1}{2}\omega_0 g^2 + \frac{7}{16}\omega_0 g^4 - t' g^4 \sum_{j=1}^{D} \left[\cos(k_j) + \cos(k'_j)\right] , \qquad (2.28)$$

where $\mathbf{k}= (k_1, k_2, ..., k_D)$ is the relative momentum of the pair. The BCS equations are:

$$\begin{aligned}
\Delta_{\mathbf{k}} &= -\frac{1}{L^D} \sum_{\mathbf{k}'} V_{\mathbf{k}\mathbf{k}'} \frac{\Delta_{\mathbf{k}'}}{2E_{\mathbf{k}'}} , \\
E_{\mathbf{k}} &= \sqrt{(\epsilon_{\mathbf{k}} - \mu)^2 + \Delta_{\mathbf{k}}^2} , \\
\epsilon_{\mathbf{k}} &= -2t' \sum_{j=1}^{D} \cos(k_j) , \\
n &= 1 - \frac{1}{L^D} \sum_{\mathbf{k}} \left(\frac{\epsilon_{\mathbf{k}} - \mu}{E_{\mathbf{k}}} \right) ,
\end{aligned}$$

being n the electron density and μ the chemical potential. The form of the BCS equations implies that the gap Δ_k depends on the wavevector $\mathbf{k}$ only through the free particle dispersion ϵ_k and this dependence is linear. Therefore Δ_k can be parametrized by the two unknowns Δ and χ:

$$\Delta_{\mathbf{k}} = \Delta \left[1 + \chi \sum_{j=1}^{D} \cos(k_j)\right] \qquad (2.29)$$

and the BCS set of equations reduce to a set of coupled equations for Δ, χ and the chemical potential μ which must be solved numerically. However, the critical line between the superconducting and the normal state can be obtained analytically by looking for a vanishing solution: $\Delta \to 0$. In the analysis of this limit of the BCS equations it is important to keep also the subleading term in $\chi \sim 2\,t'/\mu + O(\frac{1}{\log \Delta})$ in order to get the correct asymptotic result. In this way it is possible to obtain, for arbitrary dimension, a closed expression for the critical value:

$$U_1^c + \frac{3}{4}U_2^c = \frac{1}{2}\omega_0 g^2 - \frac{7}{16}\omega_0 g^4 - g^4 \mu + O(g^6). \qquad (2.30)$$

The first two terms on the right hand side represent a negative pairing energy, originating from a gain of zero–point energy upon pairing. The last term is the correlated hopping contribution $g^4\mu$, which provides an additional pairing mechanism for $n < 1$ (in fact, in this case, $\mu < 0$). This new superconducting attraction, being intersite, is favored by a large coordination number. We recall that this term is originated by the degeneracy of the

electronic band and vibronic modes and has no equivalent in a standard non degenerate polaronic model.

In order to have a complete characterization of the phase diagram of the model, in the next section, we analyze the system in the large on–site repulsion limit.

2.5 The E-e Jahn–Teller hamiltonian in the strong on site repulsion limit

The strong on–site repulsion limit of the hamiltonian (2.14), which describes the E–e model for $g \to \infty$, has been investigated by Santoro *et al.* [28]. In this section we focus our attention on the strong on–site repulsion limit of E–e model in the weak electron–phonon coupling regime.

First of all we consider the $n = 1$ case (i.e. one electron for site). The constraint that two electrons should not be allowed to simultaneously occupy the same site leads, in such a situation, to the condition that the ground state of the system should belong to the subspace of states which have exactly one electron per site.

Before deriving the effective spin hamiltonian in the case of orbital degeneracy we review briefly the same problem in the non–degenerate situation.

In the case of a single electron in a non–degenerate level the exchange interaction is determinate by the gain in energy due to virtual transition of an electron to a neighboring site. An antiparallel orientation of the spins is seen to be preferred from the energy standpoint, in fact hops of electrons with the same spin orientation are forbidden by the Pauli principle. It turns out that the effective exchange Hamiltonian is of the Heisenberg form: $H_{\text{Heis}} = \frac{2t^2}{U} \sum_{<r,r'>} \vec{S}_r \cdot \vec{S}'_r$ where $< r, r' >$ indicates nearest neighbors sites.

In the presence of a degeneracy of the orbital associated to a single atom or molecule, the physical behavior of the system significantly changes. Antiferromagnetism in the non–degenerate case was a consequence of the Pauli principle, but if each atom has a twofold–

degenerate orbital then the restrictions imposed by the Pauli principle are weaker. In such a situation the ground state of the effective hamiltonian may be more complicated than a simple Heisenberg state.

Let us consider the hamiltonian (2.12), which describes a lattice of Jahn–Teller molecules in the weak electron–phonon coupling regime. We are going to consider, at $n = 1$, the limit where the couplings U_1, U_2 and U_3 are very large compare to the hopping amplitude t' but very small with respect to the phonon excitation energy ω_0.

Practically the derivation of the effective hamiltonian follows the same approach used in the derivation of the Heisenberg model from the Hubbard model at half filling for $U \gg t$. By lifting the initial degeneracy (4^N–fold here) in second–order perturbation theory, and introducing the total spin operator $S = S_1 + S_2$ (the subscripts 1 and 2 designate the two different orbital at each atom) and the pseudo–spin τ, defined by Eq. (2.2), we find the following effective hamiltonian:

$$\begin{aligned} H_{S\tau}^{\text{eff}} &= \frac{1}{2}\left(J_S - J_T + 2J_{\pm 1}\right) \sum_{<r,r'>} \vec{S}_r \cdot \vec{S}_{r'} + \frac{1}{2}\left(3J_T - J_S\right) \sum_{<r,r'>} \vec{\tau}_r \cdot \vec{\tau}_{r'} \\ &+ \left(J_S - J_{\pm 1}\right) \sum_{<r,r'>} \tau_r^z \tau_{r'}^z + 2\left(J_T + J_S\right) \sum_{<r,r'>} \vec{S}_r \cdot \vec{S}_{r'}\, \vec{\tau}_r \cdot \vec{\tau}_{r'} \\ &+ 4\left(J_{\pm 1} - J_S\right) \sum_{<r,r'>} \vec{S}_r \cdot \vec{S}_{r'}\, \tau_r^z \tau_{r'}^z \,, \end{aligned} \tag{2.31}$$

where:

$$\begin{aligned} J_S &= \frac{2\,t'^2}{U_1 + \frac{3}{4}U_2 - \frac{1}{2}g^2\omega_0 + \frac{7}{16}g^4\omega_0}\left(1 + \frac{1}{2}g^4\right), \\ J_T &= \frac{2\,t'^2}{U_1 - \frac{1}{4}U_2 + \frac{1}{2}g^2\omega_0 - \frac{g^4}{16}\omega_0}, \\ J_{\pm 1} &= \frac{2\,t'^2}{U_3 - \frac{3}{16}g^4\omega_0}\left(1 - \frac{1}{4}g^4\right). \end{aligned} \tag{2.32}$$

J_S, J_T and $J_{\pm 1}$ are the three super–exchange couplings corresponding to the different possible states of a virtually doubly–occupied site. More precisely: J_S is related to an intermediate doubly–occupied level with $S = J_z = 0$, J_T to a virtual state with $S = 1$ and $J_z = 0$ and, finally, $J_{\pm 1}$ to a level with $S = 0$ and $J_z = \pm 1$.

Notice that in the strong electron–phonon coupling limit, $g \to \infty$, only the singlet doubly

occupied state can be involved in the virtual hopping process, leading to an effective hamiltonian of the form (2.31) with $J_T = J_{\pm 1} = 0$.

The hamiltonian (2.31) is clearly isotropic in the spin variables S, while an anisotropy is present for the terms containing the pseudo spin τ. This leads to an invariance of the model under a global $SU(2) \times U(1)$ symmetry. However for special choices of the coupling constants, further symmetries can appear. For instance when $J_S = J_{\pm 1}$ the symmetry group is $SU(2) \times SU(2)$. Moreover when $J_S = J_T = J_{\pm 1}$ the model is $SU(4)$ invariant and is a particular case of a wide class of $SU(N)$ invariant models solved by Sutherland [55]. This particular point corresponds to the situation where the levels of the two–electron multiplet become degenerate.

Another interesting limit is represented by the point $J_T = J_{\pm 1} = 0$, which we have seen to describe the E–e model in the strong electron–phonon regime. In this case the symmetry group is again $SU(4)$ [28, 56].

Notice that the absence of terms of the form $S\tau$ from (2.31) corresponds to the absence of a spin–orbit interaction.

Usually, in real systems, the exchange interaction $J_{\pm 1}$ is small compared to J_T and J_S, due to the fact that the Coulomb repulsion is stronger for electrons which occupy the same orbital. Therefore, in the following, we neglect, in the hamiltonian (2.31), the terms proportional to $J_{\pm 1}$.

An approximate phase diagram for the hamiltonian of Eq. (2.31) can be obtained by using mean field techniques. In particular we consider a Hartree–Fock factorization of the terms, in hamiltonian (2.31), which couple the spin and the pseudo spin degrees of freedom. Then by substituting the corresponding average values, $< SS >$ and $< \tau\tau >$, we find two effective hamiltonians, one for the spins S and one for the pseudo spin variables τ. The corresponding mean field solution looks like different for J_S smaller or larger than J_T. If $J_S < J_T$ the ground state is characterized by a ferromagnetic order in the spin variables and an antiferromagnetic order in the pseudo spin variables. On the other hand, for $J_S > J_T$, the ground state associated to the spin degrees of freedom becomes a Néel like state.

However, particularly in one dimension, a large value of the singlet coupling J_S may favour a valence bond ground state (which is characterized by a gap in the excitation spectrum) respect to the Heisenberg solution [28]. A simple variational calculation in $1D$ shows that a valence bond state of the form:

$$\begin{aligned} |\Psi_{VB}\rangle &= |\Psi^{(S)}_{VB}\rangle \cdot |\Psi^{(\tau)}_{VB}\rangle \\ |\Psi^{(S)}_{VB}\rangle &= \prod_{r \text{ even}} \frac{1}{2}\left[(c^\dagger_{1,r,\uparrow} c^\dagger_{1,r+1,\downarrow} - c^\dagger_{1,r,\downarrow} c^\dagger_{1,r+1,\uparrow}) + (1 \Leftrightarrow 2) \right] \\ |\Psi^{(\tau)}_{VB}\rangle &= \prod_{r \text{ even}} \frac{1}{2} \sum_\sigma \left[c^\dagger_{1,r,\sigma} c^\dagger_{2,r+1,\sigma} - c^\dagger_{2,r,\sigma} c^\dagger_{1,r+1,\sigma} \right] \end{aligned}$$

wins, for $J_S > \frac{13}{17} J_T$, over the mean field solution proposed before.

The resulting phase diagram, in one dimension, is shown in Fig 2.3.

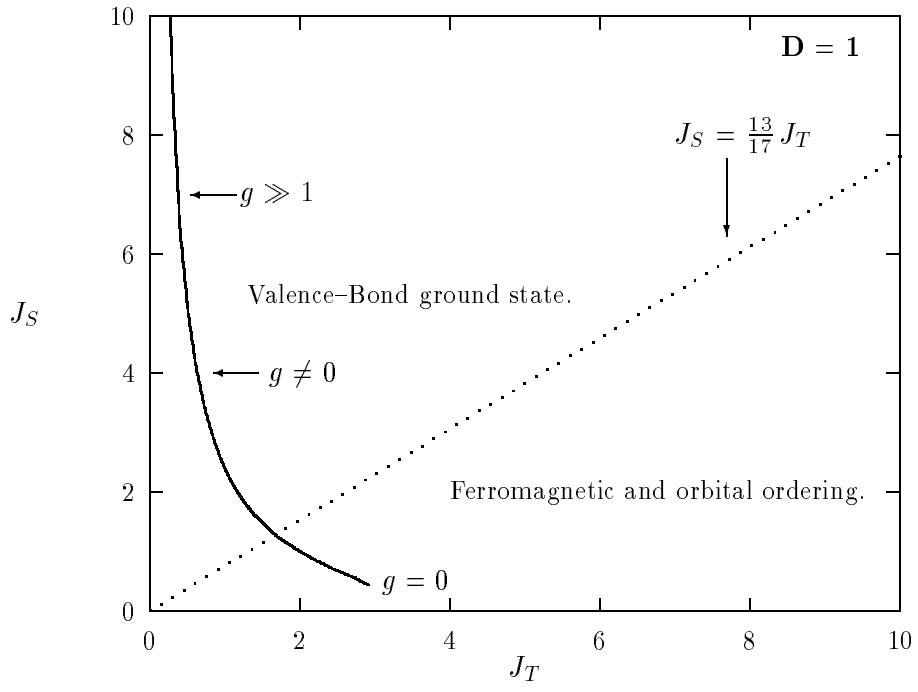

Figure 2.3: Phase diagram for the effective hamiltonian (2.31) in 1D for $J_{\pm 1} = 0$. The solid line represents the trajectory followed by the model, increasing g.

As soon as g is sufficiently large a spin (and pseudo spin) gap comes out in the excitation spectrum energy of the model. In higher dimension the competition between the Heisenberg state and the valence bond state is more delicate and an accurate numerical analysis of the model would be necessary in order to clarify this point.

Away from $n = 1$, the effective hamiltonian contains, besides the spin (and pseudospin) dependent contribution, a kinetic term, which transfers one electron from a singly-occupied site to an empty one:

$$H^{\text{eff}} = P_0 \left[-t' \sum_{a=1,2} \sum_{<r,r'>,\sigma} c^{\dagger}_{a,r,\sigma} c_{a,r',\sigma} \right] P_0 + H^{\text{eff}}_{S\tau}\,, \tag{2.33}$$

being P_0 the projection onto the subspace containing no doubly occupied sites at all.
If we assume that the polaronic attraction and the correlated hopping effect are so strong that the singlet state $S = J_z = 0$, for two electrons, is much more favored than the other levels, then one can consider $J_T = J_{\pm 1} = 0$. In such a situation, for the one dimensional version of the model, it has been shown in Ref. [24] that the spectrum of H^{eff} has a gap both in the spin and in the pseudo spin sector at all densities and the ground state for the squeezed spin chain is again a kind of valence bond state.

3 Superconducting Ground State in a Model with Bond–Charge Interaction

In this Chapter we study an Hubbard–type model with bond–charge interaction and on site repulsion U.

In Sections 3.1 we introduce the model and discuss its symmetry properties.

In Section 3.2 and 3.3 we solve the two–particle problem. This exact solution shows the presence of a bound state, both in one and two dimensions, for an Hubbard repulsion U smaller than a critical value U_c. At low density superconductivity follows from the condensation of these preformed pairs (dimers).

In Sections 3.4 and 3.5 we calculate the one dimensional correlation exponents both in the zero density limit, starting from the two and four particle solution, and at quarter filling, for several values of the parameters, by a finite–size scaling analysis.

Section 3.6 is dedicated to the BCS solution of the model in any dimension.

Finally Section 3.7 is devoted to the discussion of the phase diagram, both in one and in two dimensions.

3.1 The model and its symmetries

The hamiltonian we are going to analyze is that of a Hubbard model with correlated hopping and reads:

$$\begin{aligned} H &= -\sum_{<rr'>}\sum_{\sigma}(c^{\dagger}_{r\sigma}c_{r'\sigma}+h.c.)\,[t-\gamma\,(n_{r'-\sigma}+n_{r-\sigma})+\beta\,n_{r'-\sigma}\,n_{r-\sigma}] \\ &\quad + U\sum_{r} n_{r\uparrow}\,n_{r\downarrow}\,. \end{aligned} \tag{3.1}$$

The interaction term includes the on–site Coulomb repulsion U and the bond–charge interactions γ and β, which describe an enhanced hopping amplitude for particles in doubly occupied sites. The number operator for electrons of spin σ on a site r is denoted by $n_{r\sigma}=c^{\dagger}_{r\sigma}c_{r\sigma}$.

The model described by the hamiltonian (3.1) contains the model proposed by Hirsch and Marsiglio in the particular case of $\beta=0$ [35, 36, 37, 38]. Also a model of the some form was obtained in Ref. [45] as effective one band model resulting from tracing out the degrees of freedom associated to the oxygen electronic band in cuprates.
Exact solutions for special choices of the parameters have been recently obtained in similar 1D models [33, 34, 57, 58].

The hamiltonian (3.1) has the usual SU(2) spin symmetry (the total spin is conserved) and the U(1) charge symmetry (due to conservation of the charge) but also other additional symmetries can be found for particular values of the coupling constants.
Under a "particle–hole" transformation of the form $\tilde{c}_{r,\sigma}=c^{\dagger}_{r,\sigma}(-1)^{r}$ (where we have supposed that the model is defined on a bipartite lattice) the parameters of the hamiltonian (3.1) change as:

$$\begin{aligned} \tilde{t} &= t-2\gamma+\beta\,, \\ \tilde{\gamma} &= -\gamma+\beta\,, \\ \tilde{\beta} &= \beta\,, \end{aligned} \tag{3.2}$$

the symbol $\tilde{}$ indicates transformed parameters or operators. From relations (3.2) one

concludes that the hamiltonian (3.1) retains the same form under this symmetry only in two cases: for $\beta = 2\gamma$, which include the Hubbard limit ($\gamma = \beta = 0$), and for $\gamma = t$ and $\beta = 0$.

A new symmetry transformation, which requires to allow $\gamma \neq 0$ and $\beta \neq 0$ is:

$$\tilde{c}_{r,\sigma} = (1 - 2n_{r,-\sigma})\, c_{r,\sigma}\,. \tag{3.3}$$

It is equivalent to change the phase of $c^{\dagger}_{r\uparrow} c^{\dagger}_{r\downarrow}|0>$ by a factor -1. Under this transformation the parameters t, γ and β must change according to the following relations:

$$\begin{aligned} \tilde{t} &= t\,, \\ \tilde{\gamma} &= -\gamma + 2t\,, \\ \tilde{\beta} &= \beta + 4(t - \gamma)\,. \end{aligned} \tag{3.4}$$

When $\gamma = t$ the transformation (3.3) becomes a symmetry of the model and the number of doubly occupied sites is conserved. An enlarged symmetry occur when $\gamma = t$ and $\beta = 0$, where the model possesses an additional SU(2) symmetry, with generators:

$$\eta^{-} = \sum_{r} c^{\dagger}_{r\uparrow} c^{\dagger}_{r\downarrow}\,, \qquad \eta^{+} = (\eta^{-})^{\dagger}\,, \qquad \eta_z = \frac{1}{2}\sum_{r}(1 - n_r)\,. \tag{3.5}$$

In this case an exact solution can be provided. More precisely, the exact ground–state wave function and energy, at half filling and in arbitrary dimension, has been found by Vollhardt in Ref. [57], while in one dimension the model has been solved exactly, for arbitrary filling, by Arrachea and Aligia in Ref. [58]. Note that the above generators are just those of pseudospin corresponding to hidden SU(2) symmetry of the ordinary Hubbard model.

Another particular point is for $\beta = 2\gamma = 2t$. Also in this case an additional SU(2) symmetry is found, with generators:

$$\eta^{-} = \sum_{r} (-1)^{r} c^{\dagger}_{r\uparrow} c^{\dagger}_{r\downarrow}\,, \qquad \eta^{+} = (\eta^{-})^{\dagger}\,, \qquad \eta_z = \frac{1}{2}\sum_{r}(1 - n_r)\,. \tag{3.6}$$

In the following sections we mainly focus our attention on two simple parameter choices: *i)* $\beta = 0$, i.e. keeping only terms with at most four fermion operators, and *ii)* $\beta = \gamma^2/t$

where the interaction acquires a particular symmetrical form and can be easily interpreted as a tight binding model with a density dependent hopping amplitude:

$$t \;\rightarrow\; t\,(1 \,-\, \frac{\gamma}{t}\,n_{r\,-\sigma})\,(1 \,-\, \frac{\gamma}{t}\,n_{r'\,-\sigma})\,. \tag{3.7}$$

3.2 The two–particle problem

We first address the problem of few particles in vacuum by reviewing the exact solution of two-body problem in arbitrary dimension which was investigated by Marsiglio and Hirsch [59].

Let us consider two electrons: In this case the β term in the hamiltonian is ineffective and can be dropped. A generic state in the Hilbert space with total z-component of the spin equal zero, can be written as:

$$|\Psi\rangle \;=\; \sum_{r,r'} \;\psi(r,r')\,c^{\dagger}_{r\uparrow}\,c^{\dagger}_{r'\downarrow}\;|0\rangle\;, \tag{3.8}$$

where the vacuum $|0\rangle$ is the state without electrons.

The Schrödinger equation is easily solved in momentum space where the wavefunction of the singlet spectrum has the form:

$$\psi_k \;=\; A \,+\, \frac{B}{E \,-\, \epsilon_k \,-\, \epsilon_{P-k}}\,, \tag{3.9}$$

P is the total momentum of the state, ϵ_k is the tight-binding dispersion of the free-electron problem ($\epsilon_k = -2t\sum_{j=1}^{D}\cos k_j$) and the two constants A and B are related to the value of the wavefunction at $r - r' = 0$ ($\psi(0)$) and at nearest neighbors ($\psi(\pm 1)$):

$$\begin{aligned} A \;&=\; \frac{\gamma}{t}\,\frac{1}{\sqrt{L^D}}\,\psi(0)\,, \\ B \;&=\; \frac{1}{\sqrt{L^D}}\left\{\left(U - E\frac{\gamma}{t}\right)\psi(0) + 2\gamma\,[\psi(1)+\psi(-1)]\right\}\,. \end{aligned}$$

By imposing the self–consistency condition, we obtain the eigenvalue equation for the energy E in arbitrary spatial dimension:

$$\frac{1}{L^D}\sum_{k}\frac{1}{E \,-\, \epsilon_k \,-\, \epsilon_{P-k}} \;=\; \frac{(\gamma - t)^2}{E\,\gamma\,(\gamma - 2\,t) \,+\, U\,t^2}\,. \tag{3.10}$$

Remarkably this eigenvalue equation is identical to that of the Jahn–Teller model (Eq. (2.22), which we have studied in Section 2.3) by relating the parameters of the two models through the following equation:

$$\gamma = \left[1 - \sqrt{2}\, r(g)\right] t' \,. \tag{3.11}$$

and by identifying t' with t. This surprising result is a consequence of the fact that a complete and rigorous mapping between the two models can be established in the case of two particles, including all states. In order to construct this mapping, the first step is to connect the two Hilbert spaces, associated to the bond–charge model and the E–e model respectively, through a one to one correspondence. The main difficulty in order to do that is related to the different dimensions of the two Hilbert spaces. In fact the two–particle Hilbert space, with total z–component of the spin equal zero, for a non degenerate purely electronic model, $\mathcal{H}^{BC}$, has a dimension given by L^2, where L is the size of the lattice. On the other hand, the dimension of the two–particle Hilbert space, with total z–component of the spin and pseudospin equal zero, for a lattice of Jahn–Teller molecules is given by $2 \times L^2$ in the weak electron-phonon coupling limit and by $2 \times L^2 - L$ in the strong coupling regime (the factor 2 is a consequence of the orbital degeneracy). However the ground state of the E–e Jahn–Teller hamiltonians (2.12,2.14) belongs to the sub–space of singlet states (respect to the pseudo spin variables), and this sub–space, $\mathcal{H}^{E-e}_{SING}$, is closed respect to the action of the hamiltonians (2.12,2.14). This suggest considering the mapping only between the sub–space of singlet states, $\mathcal{H}^{E-e}_{SING}$, and the full Hilbert space, $\mathcal{H}^{BC}$, associated to the bond–charge model. The one to one correspondence, which realizes the equivalence between the two models, is given by:

$$\frac{1}{\sqrt{2}} \left(c^\dagger_{r,1,\uparrow} c^\dagger_{r',2,\downarrow} + c^\dagger_{r,2,\uparrow} c^\dagger_{r',1,\downarrow} \right) |0\rangle \iff c^\dagger_{r\uparrow}\, c^\dagger_{r'\downarrow}\, |0\rangle \,, \tag{3.12}$$

in the weak electron–phonon coupling limit, and by:

$$\frac{1}{\sqrt{2}} \left(S^+_r S^-_{r'} + S^-_r S^+_{r'} \right) c^\dagger_{r,\uparrow} c^\dagger_{r',\downarrow} |0\rangle \iff c^\dagger_{r\uparrow}\, c^\dagger_{r'\downarrow}\, |0\rangle \,, \tag{3.13}$$

at strong coupling.

It is matter of algebra to verify that the matrix elements of the bond–charge hamilto-

nian (3.1) and the E–e Jahn–Teller hamiltonians (2.12,2.14) coincide when the parameters γ and g satisfy the relation (3.11).

It is worth mentioning that the mapping between the two models cannot be extended beyond the two–particle case. In fact the orbital degeneracy present in the E–e hamiltonian increases considerably the dimension of the Hilbert space associated to the system respect to a non–degenerate model. For instance, in a lattice of L sites with four electrons, the dimension of the sub–space of singlet states, $\mathcal{H}^{E-e}_{SING}$, associated to the E–e model reads:

$$\mathcal{D}(\mathcal{H}^{E-e}_{SING}) = \left[2 + O\left(\frac{1}{L}\right)\right] \mathcal{D}(\mathcal{H}^{BC}) \,, \tag{3.14}$$

being $\mathcal{D}(\mathcal{H}^{BC})$ the dimension of the hilbert space in the non degenerate case. It is therefore clear that a mapping between the two Hilbert spaces, $\mathcal{H}^{E-e}_{SING}$ and $\mathcal{H}^{BC}$, is impossible for more than two electrons.

As a consequence of the mapping (3.12,3.13), the results obtained in Section 2.3, for the two–particle problem, can be transferred to the context of the bond–charge model. It turns out that Eq. (3.10) has a bound state for $\gamma < 0$ both in one and two dimensions, at every value of the total momentum P and even for repulsive $U > 0$, up to

$$U_c = 4\,D\,\gamma\,\left(\frac{\gamma}{t} - 2\right) \tag{3.15}$$

for $D \leq 2$. So, a finite, positive $U > U_c$ is needed in order to destroy the bound pair. Remarkably, the rather strong attraction responsible for this binding is generated by the bond–charge interaction alone. The binding mechanism involves a gain in kinetic energy when two particles are at nearest neighbor distance. This interpretation is supported by the form of the wavefunction which is peaked not just on site but also at the nearest neighbors, while decreasing exponentially elsewhere. The critical U_c increases in going from one to two dimensions because of the enhanced efficiency of the bond–charge interaction which grows when the number of nearest neighbors increases. The absolute ground state is always in the $P = 0$ sector and the presence of a bound state for any total momentum P is easily interpreted as describing a coherent motion of the bound pair. At larger values of U double

occupancies are suppressed inhibiting the mechanism leading to binding: The pair breaks and the low energy spectrum is continuous.

3.3 Two, three and four particle bound state in $D = 1$

For two particles, in $D = 1$, the analytical solution of the eigenvalue equation (3.10) can be worked out immediately using the mapping (3.11,3.12, 3.13) and the results obtained in Section 2.3 (Eqs. (2.24), (2.25) and (2.26)): the ground state energy, in the thermodynamic limit, is given by

$$E_b(P) = \frac{U\gamma(\gamma - 2t) - (\gamma - t)^2 \sqrt{U^2 + 8\,(1 + \cos P)(t^2 - 4\gamma t + 2\gamma^2)}}{t^2 - 4\gamma t + 2\gamma^2} \tag{3.16}$$

and the corresponding bound pair wavefunction reads:

$$\psi(r - r') = \psi(0) \left[(1 - \frac{\gamma}{t})\, e^{-\lambda\,|r - r'|} + \frac{\gamma}{t} \delta_{r,r'} \right] \tag{3.17}$$

for total momentum $P = 0$. Here, the size of the pair $1/\lambda$ is a function of the parameters γ and U and diverges along the critical line (3.15):

$$\lambda = -\log \left[\frac{t}{4} \frac{U + \sqrt{U^2 + 16\,(t^2 - 4\gamma t + 2\gamma^2)}}{t^2 - 4\gamma t + 2\gamma^2} \right] . \tag{3.18}$$

As previously discussed, an attraction between pairs in vacuum may lead either to superconductivity or to phase separation according to the form of the *residual interaction* once the pair is formed. The best way to investigate the sign of this residual interaction is via a direct calculation of the ground state energy of a system of three and four particles. Contrary to the case of two particles, this problem cannot be solved exactly, even in one dimension, and we will resort to a perturbative treatment in the limit $U \to -\infty$ where the pair is strongly bound on site. These perturbative results will be later confirmed by a numerical calculation for four particles at $U = 0$ in $D = 1$.

Let us consider first the three–particle problem at $\beta = 0$. The negative U Hubbard model is known, from the Bethe ansatz solution, to show no three–particle bound state, due to

the saturation of the attractive interaction when a pair is placed on the same site. The bond–charge interaction deeply modifies this scenario leading to a three–particle bound state, at least for large, negative U.

Let us consider three electrons in the subspace of total momentum $P = 0$. The generic wave function can be written as:

$$|\Psi\rangle = \sum_{r,r',r''} \psi(r,r',r'')\, c^{\dagger}_{r\uparrow}\, c^{\dagger}_{r'\downarrow}\, c^{\dagger}_{r''\uparrow}\, |0\rangle\,. \tag{3.19}$$

The Schrödinger equation, in k–space is easily shown to be

$$\Psi(-p,k+p,-k) = A(k) - A(p) + \frac{B(k)-B(p)}{E-\epsilon_k-\epsilon_p-\epsilon_{k+p}} \tag{3.20}$$

where:

$$\begin{aligned} A(k) &= \frac{\gamma}{t}\frac{1}{L}\sum_p \Psi(-p,k+p,-k)\,, \\ B(k) &= \left(U\frac{t}{\gamma} - E + \epsilon_k\right) A(k) - \frac{\gamma}{t}\frac{1}{L}\sum_p (\epsilon_p + \epsilon_{k+p})\, \Psi(-p,k+p,-k)\,. \end{aligned}$$

For large, negative U, the perturbative expansion of Eq. (3.20) gives the ground state energy:

$$E = U\ - 2t\,\frac{1+(1-\frac{2\gamma}{t})^2}{2(1-\frac{2\gamma}{t})} + \frac{1}{U}\left[12\,t^2\,\frac{(1-\frac{\gamma}{t})^4}{(1-\frac{2\gamma}{t})^2} - 4\,t^2\,\frac{(1-\frac{\gamma}{t})^4}{(1-\frac{2\gamma}{t})^4}\right] + O\left(\frac{1}{U^2}\right)\,. \tag{3.21}$$

The corresponding wavefunction represents a three-body bound state:

$$\Psi(r,r',r'') = \frac{1}{2}\sqrt{\frac{\gamma}{t}\left(\frac{\gamma}{t}-1\right)}\left[\delta_{r',r''}\,\mathrm{sign}(\mathrm{r}'-\mathrm{r})\,e^{-\phi|r'-r|} - \delta_{r',r}\,\mathrm{sign}(\mathrm{r}'-\mathrm{r}'')\,e^{-\phi|r'-r''|}\right] + O(\frac{1}{U})\,,$$

where $\phi = \log(1-\frac{2\gamma}{t})$. The form of the ground state energy (3.21) suggests that, when attraction is weakened, the three–particle bound state becomes unstable against breaking into one dimer and one free particle. The critical value $U_c^{(3)}$ for this transition can be estimated by our strong coupling expansion as:

$$U_c^{(3)} = -2\,t\,\left(1-\frac{\gamma}{t}\right)^2\,\frac{10(\frac{\gamma}{t})^2 - 14\frac{\gamma}{t} + 5}{(1-\frac{2\gamma}{t})^3} \tag{3.22}$$

which is shown in Fig. 3.1 as a function of the parameter γ. The problem is now to

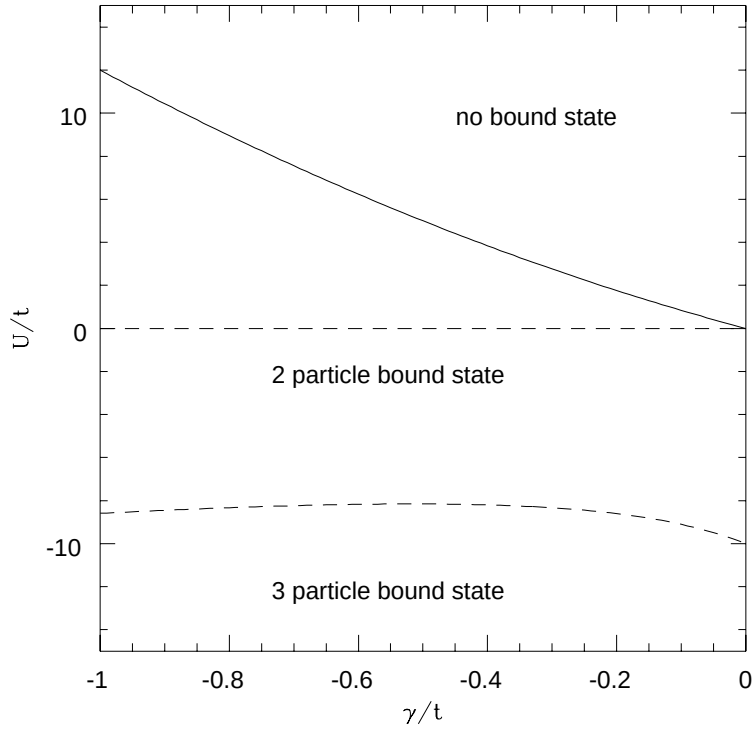

Figure 3.1: Zero temperature phase diagram for three particles. Notation as in the text.

understand whether the bound state survives for more than three particles leading to phase separation or not. In order to investigate this question, we consider the four–electron problem, again in the limit of large, negative U. On general grounds, the perturbative expansion in $1/U$ of the ground state energy has the form:

$$E(4) = 2\,U + \frac{\alpha}{U} + O\left(\frac{1}{U^2}\right) , \tag{3.23}$$

where α is the eigenvalue of the effective hamiltonian of the model for $U \to -\infty$, $H_{\rm eff} = \frac{1}{U} P_2\, H^2\, P_2$. P_2 is the projection operator on the Hilbert space with double occupancies. The possible formation of a four–particle bound state crucially depends on the sign of α. By writing the corresponding Schrödinger equation it is easy to obtain a self–consistent

equation for α:

$$\frac{1}{L}\sum_k \frac{1+\cos(k)}{1-\frac{\alpha}{8\,(\gamma-t)^2}+\cos(k)} = 0\,, \tag{3.24}$$

whose solution can be found analytically in 1D:

$$\alpha = 8\,(\gamma-t)^2\left(2-\frac{\pi^2}{2L^2}\right)\,. \tag{3.25}$$

By use of this result, the binding energy of the four particle system $\Delta E = E(4) - 2E(2)$ can be explicitly evaluated to order $1/U$:

$$\Delta E = E(4) - 2\,E(2) = \frac{(\gamma-t)^2}{|\,U\,|}\,\frac{4\,\pi^2}{L^2} + O\left(\frac{1}{U^2}\right)\,. \tag{3.26}$$

Note that the binding energy is positive and vanishes in the thermodynamic limit. This provides a strong indication for the absence of bound states involving more than two particles and suggests that the model, in the low density regime, behaves as a dilute gas of dimers which are characterized by a weak repulsive residual interaction. These composite particles are characterized by their effective mass which can be evaluated through the momentum dependence of the two–particle ground state energy $E_b(P)$ (3.16). At large negative U and (small) total momentum P, $E_b(P)$ can be expanded as [60] $E(P) = E_0 + t_{eff}\,P^2$ where the dimer hopping amplitude is $t_{eff} = -2\,(\gamma-t)^2/U$. This result is entirely compatible with a picture of dimers behaving as a gas of hard core bosons with effective hopping amplitude t_{eff}. In fact, the representation in terms of free hard core bosons would imply a zero point kinetic energy $t_{eff}\,2\pi^2/L^2$ which agrees with the four particle perturbative result (3.26) via the definition of t_{eff}. This fact gives confidence on the picture of the low density regime as a dimer gas and allows to extend the definition of the effective hopping amplitude for dimers by use of Eq. (3.16) at arbitrary $U < U_c$:

$$t_{eff} = \frac{2\,(t-\gamma)^2}{\sqrt{U^2 + 16\,(t^2 - 4\,\gamma\,t + 2\gamma^2)}}\,. \tag{3.27}$$

In order to provide a check on expression (3.27) and to confirm the superfluid dimer picture, we can solve the four–particle problem at $U = 0$ by exact diagonalization of the hamiltonian (3.1). The zero point kinetic energy of the four particles ΔE is numerically evaluated in

1D rings as:

$$\Delta E = E(4, L) - 2\,E(2, \infty) = \frac{2\,\pi^2}{L^2}\,t_{eff}\,. \tag{3.28}$$

The finite size scaling of the numerical results is shown in Fig. 3.2 for two different values of γ and $\beta = \gamma^2/t$. It proves that ΔE is positive and vanishes in the thermodynamic limit (i.e. the four particles do not form a bound state). Moreover, the asymptotic behavior of ΔE as $L \to \infty$ agrees with the theoretical value obtained via Eq. (3.27), also shown in figure. In conclusion we can state that the model is stable against phase separation. The

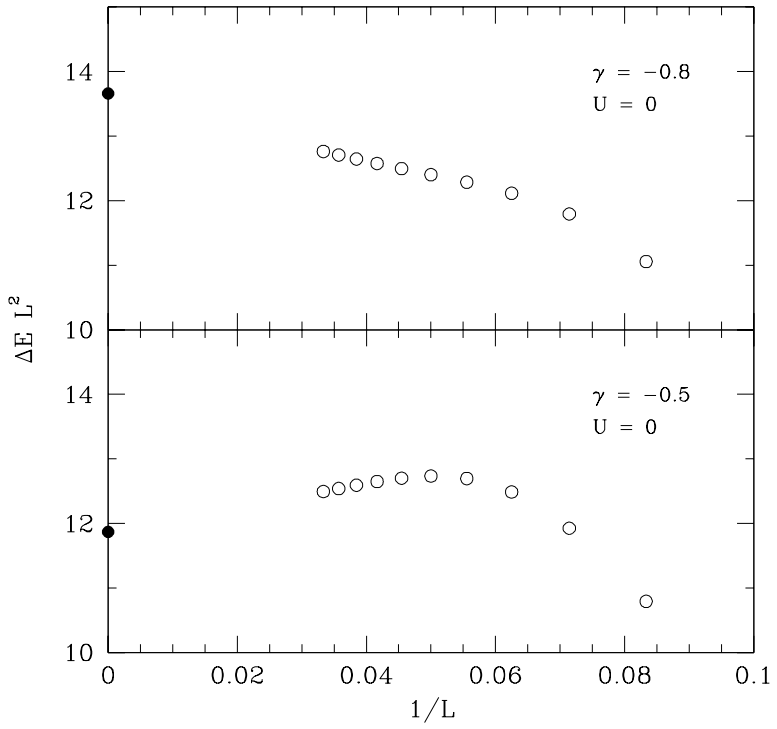

Figure 3.2: Size scaling of the ground state energy of the hamiltonian in Eq. (3.1) with $U = 0$ and four electrons for two different value of parameter γ. $\Delta E = E(4, L) - 2E(2, \infty)$ where $E(N, L)$ is the ground state energy of N electrons in a L-site ring in units of t. The full circle is the theoretical value for two hard-core bosons in the infinite lattice with t_{eff} given by equation (3.27).

system behaves as a dilute gas of dimers, which follow boson statistics and can be treated as hard core particles. Therefore it is quite plausible that, at least at low density, the ground state is a superconductor via Bose condensation of pre–existing pairs. This result is rather robust against the presence of Hubbard repulsion U and a remarkably large value of $U > 0$ is needed to break these pairs. Of course in 1D the quantum fluctuations prevent actual Bose condensation and only a ground state with power law superconductive correlations and diverging susceptibility is expected.

Notice that this physical picture of the ground state of the bond–charge model as a dilute gas of dimers is quite similar to that given for the E–e Jahn–Teller model in the low density limit (see Section 2.3). Therefore, although an exact mapping between the bond–charge model and the E–e model can be carried out only for the two–particle case, the superconducting properties of the two systems, at low density, coincide.
On the opposite hand the properties of the normal state in the bond–charge model and in the E–e Jahn–Teller model are significantly different. In fact for the bond–charge hamiltonian an ordinary Luttinger liquid without spin gap is present above U_c (see next section for a more detailed discussion about this point) while in the E–e hamiltonian, at least for g sufficiently large, the spin (and also the pseudo spin) degrees of freedom are gapped and only the charge degrees of freedom remain gapless (see Section 2.5).

3.4 Correlation exponents in 1D: Zero–density limit

In this section we focus on the 1D model where considerable progress in the understanding of the physical properties of the system can be gained by use of the powerful theoretical techniques of conformal field theory [61]. In particular, we will show how the exact solution for two and four particles previously discussed, can be used to evaluate analytically the correlation exponents in the zero density limit. Then, we will evaluate the critical exponents for several choices of the parameters at quarter filling by a finite size scaling analysis.

The behavior of the model at low density appears to be markedly different for U smaller or larger than its critical value U_c (3.15). In the former case, the analysis of the two–particle problem shows that a spin gap is present in the excitation spectrum of the model, and thus we expect that the spin–spin correlations decay exponentially. On the other hand, the charge excitation spectrum is expected to remain gapless, as shown by the absence of four–particle bound states. In this case, the model should fall in the universality class of the Luther–Emery model [62] and its correlation exponents are expressed in terms of the unique parameter K_ρ [63]. This exponent can be related to the compressibility of the model using the Haldane–Schulz equation:

$$L\frac{\partial^2 E}{\partial N^2} = \frac{\pi}{2}\frac{u_\rho}{K_\rho} \,, \tag{3.29}$$

where u_ρ is the charge velocity of the system, which is associated to the long wavelength charge excitations: $E_k \sim u_\rho k$. In particular, the long distance behavior of the charge correlations at $2\,k_F$ is $C_\rho(r) \sim \cos(2k_F r)/r^{K_\rho}$ while the s–wave superconductive correlations decay as $\Delta(r) \sim r^{-1/K_\rho}$. The Luther Emery model is characterized by a central charge $c = 1$ which is related to the leading finite size corrections of the ground state energy:

$$\frac{E}{L} = e_\infty - c\,\frac{\pi\, u_\rho}{6L^2} \,. \tag{3.30}$$

In the other regime, for $U > U_c$ (3.15), the bound state is not present anymore and both the spin and charge excitations are gapless, at least away from half filling, where Umklapp processes are absent. This can be also checked by going to the $U \to \infty$ limit where the bond–charge model maps into a standard $t - J$ model with $J = 4(t-\gamma)^2/U$. The $t - J$ model at small J is known to be a Luttinger Liquid [30] whose correlation exponents are again parametrized by K_ρ (3.29). In this case, all the correlation functions of the model are characterized by a power law behavior: Both the spin and charge correlations at $2k_F$ decay as r^{-1-K_ρ} while the charge correlations at $4k_F$ fall as r^{-4K_ρ}. Also the Luttinger Liquid is characterized by a central charge $c = 1$, but, in this case, the presence of long wavelength gapless spin excitations modifies Eq. (3.30) into:

$$\frac{E}{L} = e_\infty - c\,\frac{\pi\,(u_\rho + u_\sigma)}{6L^2} \,, \tag{3.31}$$

where u_σ is the spin velocity.

This field theoretical formalism allows for the analytical evaluation of the correlation exponents of our model in the zero density limit, where use can be made of the exact results obtained for few particles in a finite system. The key assumption, explicitly verified in the Hubbard model where Bethe Ansatz solution is also available, is that the zero density limit of the physical properties of the model is correctly reproduced by fixing the total number N of particles in the system at a given lattice size L and then taking the $L \to \infty$ limit. Following this procedure, the ground state energy of two and four particles at $U < U_c$ can be written as:

$$E = E_b \frac{N}{2} + \frac{\pi^2}{24} t_{eff} \frac{N^3}{L^2} - \frac{\pi^2}{6} t_{eff} \frac{N}{L^2} + O(L^{-3}) ; \tag{3.32}$$

here use has been made of Eqs. (3.16, 3.28). The charge velocity can be obtained by the $1/L$ expansion of the energy of a pair at total momentum $P = 2\pi/L$, which, via Eq. (3.27), is:

$$u_\rho = \pi \frac{N}{L} t_{eff} . \tag{3.33}$$

Equations (3.29), (3.32) and (3.33) give the zero density limit of the K_ρ exponent at all $U < U_c$ (3.15): $K_\rho = 2$ independent of U coinciding with the negative U Hubbard model result. Also the central charge c of the system can be calculated by use of Eqs. (3.32, 3.33, 3.30). The resulting value for c is $c = 1$, which provides a consistency test of the method used. Therefore we can conclude that the system is in the Luther Emery regime with a spin gap and diverging superconductive susceptibility. Remarkably, the critical exponents associated with the charge degrees of freedom are identical with those of a hard core boson gas, as expected from the physical picture of a dilute dimer gas.

At $U > U_c$, the one and two particle solution is sufficient to give the exact scaling of the energy and charge velocity as $L \to \infty$:

$$E = -4t + \frac{\pi^2}{3} t \frac{N^3}{L^2} - \frac{\pi^2}{3} t \frac{N}{L^2} + O(L^{-3}) , \tag{3.34}$$

$$u_\rho = 2\pi \frac{N}{L} t . \tag{3.35}$$

These expressions give $K_\rho = 1/2$ and central charge $c = 1$ showing that the system is in the Luttinger liquid regime with correlation exponents identical to those of the $U \to \infty$ repulsive Hubbard model.

To summarize, the bond–charge model is characterized by two different phases in the low density limit: a Luttinger liquid regime for $U > U_c$ with both charge–density wave and spin–density wave long range correlations at $2k_F$; a Luther–Emery phase dominated by superconductive fluctuations is instead present at $U < U_c$.

3.5 $D = 1$ at finite density

In order to understand whether the transition found at U_c for low density persists also at finite density n, we can make use of the weak coupling Renormalization group method [62] which is known to give the correct scaling and the exact critical exponents to leading order in the interaction parameters U/t and γ/t. In this case we set $\beta = 0$ so that the resulting hamiltonian is quartic in fermion operators. The model is first linearized around the two Fermi points giving rise to a general, spin isotropic, *g–ology* model with coupling constants $g_1, ..g_4$ functions of the two physical parameters U/t and γ/t. The Renormalization Group equations are then integrated and the weak coupling phase diagram is obtained [64]. The correct result can be also obtained by noticing that, linearizing both interactions around the Fermi points, we get an effective Hubbard model with coupling constant $U_{eff} = U + 8\gamma\cos(\pi \mathrm{n}/2)$. In the Hubbard model, the phase boundary between the Luttinger Liquid and the Luther Emery phase (with long range superconductive correlations) is known to be at $U_{eff} = 0$ leading to the weak coupling result:

$$U_c(\mathrm{n}) = -8\gamma\cos(\pi \mathrm{n}/2) + O(\gamma^2) \tag{3.36}$$

and the correlation exponents can be read–off the known Hubbard results [61]:

$$K_\rho = 1 - \frac{U + 8\gamma\cos(\pi \mathrm{n}/2)}{4\pi\, t\, \sin(\pi \mathrm{n}/2)} + O(U^2, \gamma^2)\,. \tag{3.37}$$

In order to go beyond a perturbative determination of the phase diagram, we have analyzed the properties of the model at quarter filling where an accurate finite size scaling can be done. We have studied in detail the case $\beta = \gamma^2/t$. A first qualitative hint on the existence of the transition comes from the analysis of the symmetries of the ground state when boundary conditions corresponding to "open shells" in the non interacting regime are chosen. In this case, the interaction is responsible for the splitting of the singlet–triplet degeneracy of the free fermion limit, and in fact two different symmetries are found, according to the choices of the parameters. If γ is negative and U is sufficiently small, the ground state is always a singlet belonging to the totally symmetric sector, as expected from the picture of a Bose condensate of s–wave Cooper pairs. Instead, by increasing U, a level crossing is observed and the ground state is a triplet, odd under reflections. This sort of "Hund rule" has been already observed in the repulsive Hubbard model for fillings corresponding to "open shell" conditions [65]. We can tentatively associate the occurrence of the transition to the choice of parameters corresponding to this level crossing. Lanczos diagonalizations have been performed for 1D lattices of 8, 12 and 16 sites with periodic (8 and 16) or antiperiodic (12) boundary conditions in order to achieve the "open shell" condition. The size scaling of the spin gap, i.e. the difference between the lowest spin singlet state and the lowest triplet state, is shown in Fig. 3.3 together with a parabolic extrapolation to the thermodynamic limit. The data strongly suggest that the gap remains finite in all the cases where the ground state is a singlet (full symbols) while if the ground state is a triplet (open symbols) the gap is seen to scale to zero in the thermodynamic limit. Similar conclusions can be drawn by the inspection of the density and magnetic structure factors. Two typical examples are shown in Fig. 3.4 for 8 electrons in 16 sites with antiperiodic boundary conditions and $\gamma = -0.5\,t$. The $U = 0$ case is characterized by a smooth magnetic structure factor, while the density correlations have a cusp at wavevector $2\,k_F$. This suggests that the spin degrees of freedom are gapped while charges are gapless and their correlations behave as at the Luther–Emery fixed point. This has to be contrasted with the behavior shown at $U = 8$ where also spin structure factor shows a cusp at $2\,k_F$

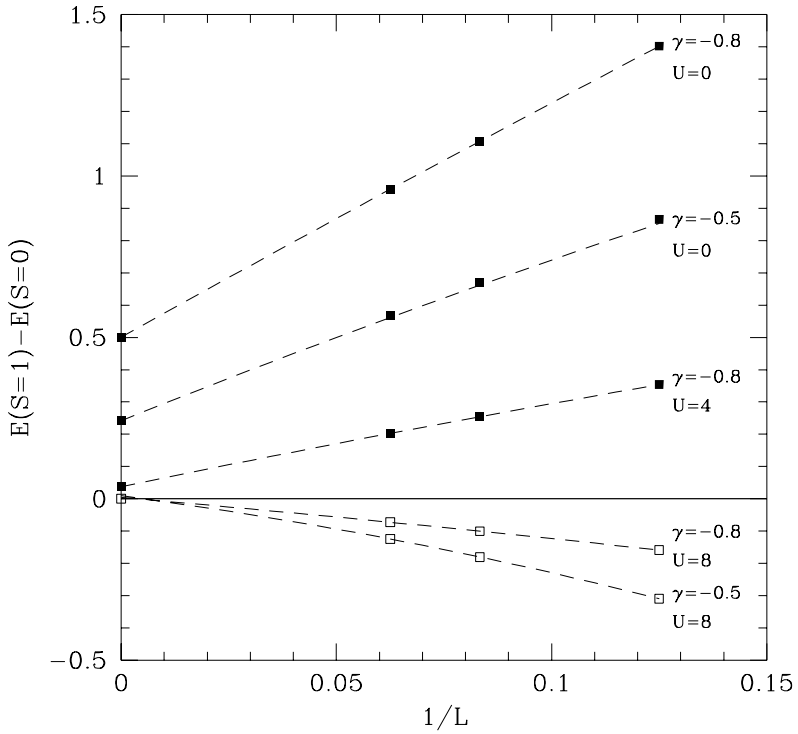

Figure 3.3: Size scaling of the spin gap from Lanczos diagonalization in 1D at quarter filling. Boundary conditions correspond to open shells. Parameters are in units of t. Full squares scale to a finite spin gap. Open squares scale to zero gap.

while the singularity of charge correlations is considerably reduced. The shape of these correlation functions is quite similar to that of the Hubbard model [66] where both spin and charge degrees of freedom are gapless and the model scales to the Luttinger fixed point.

In order to be fully quantitative in the determination of the properties of the model, use can be made of the field theoretical expression (3.29) relating the correlation exponent K_ρ to easily computable quantities, like compressibility and charge velocity. The numerical

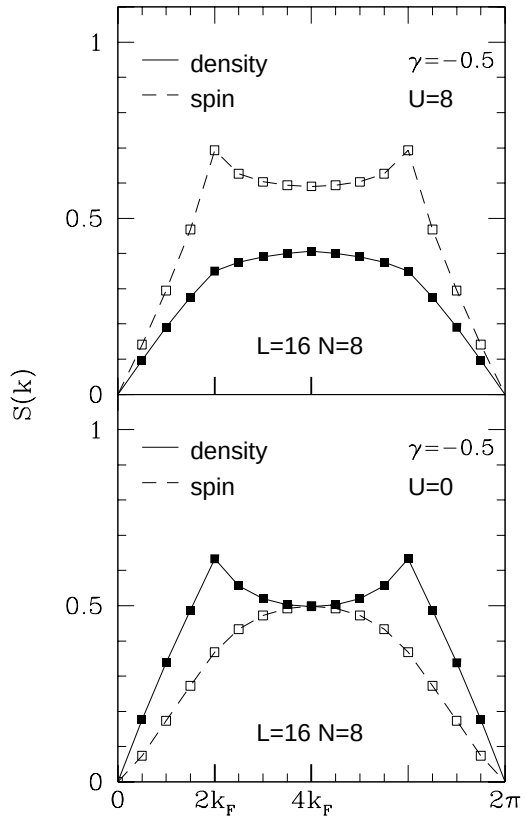

Figure 3.4: Density and spin structure factors for two parameter choices in 1D at quarter filling.

evaluation of these quantities in a finite system can be straightforwardly obtained by:

$$\begin{aligned} \frac{\partial^2 E}{\partial N^2} &= \frac{E(N+2) - 2\,E(N) + E(N-2)}{4}\,, \\ u_\rho &= \frac{L}{2\pi}\left[E\left(P = \frac{2\pi}{L}\right) - E\,(P=0)\right]\,. \end{aligned} \tag{3.38}$$

Computations have been performed at quarter filling by use of "closed shell" boundary conditions (i.e. periodic for 12 sites and antiperiodic for 8 and 16 sites). In Figs. 3.5 and 3.6, we present the size scaling for the compressibility and the charge velocity for different values of U and γ obtained via Eq. (3.38) and a parabolic extrapolation to the thermodynamic limit. The resulting K_ρ is shown in the Tables 3.1 and 3.2 where we have

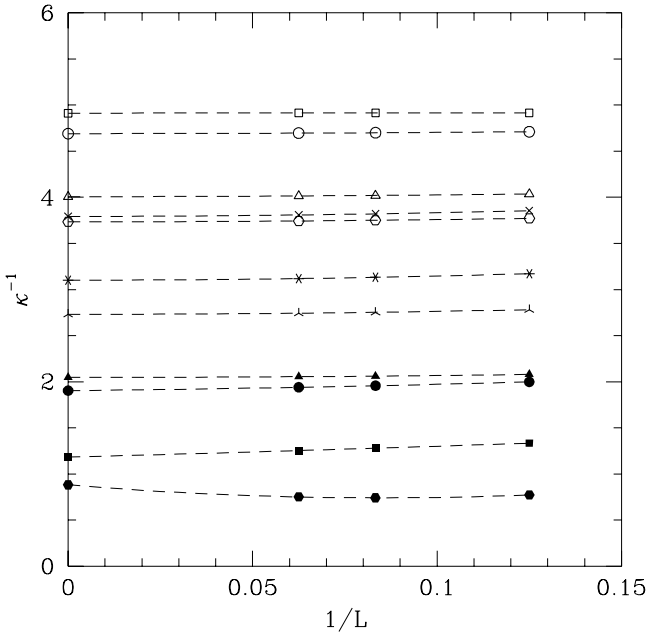

Figure 3.5: Size scaling of the compressibility in $D = 1$ at quarter filling for different parameter choices of (γ, U) (in units of t): (0,4) (open triangles); (0,8) (open squares); (-0.1,0) (full triangles); (-0.1,4) (open hexagons); (-0.1,8) (open circles); (-0.5,0) (full squares); (-0.5,4) (skeletal triangles); (-0.5,8) (crosses); (-0.8,0) (full hexagons); (-0.8,4) (full circles); (-0.8,8) (asterisks). The points at $L = \infty$ are obtained by a parabolic extrapolation of the Lanczos data.

distinguished between parameters corresponding to a $K_\rho < 1$ (Luttinger Liquid, Table 3.1) and $K_\rho > 1$ (Luther Emery, Table 3.2). For $U = 0$ the system is always in the (quasi) superconducting region in agreement with the expectations, but superconductivity gets less and less robust for density approaching half filling.

3.6 Mean Field Solution

The Hubbard model with correlated hopping was studied within BCS Mean Field approximation in 2 and 3 dimensions by Hirsch and Marsiglio [35, 36, 37, 38]. In order to compare

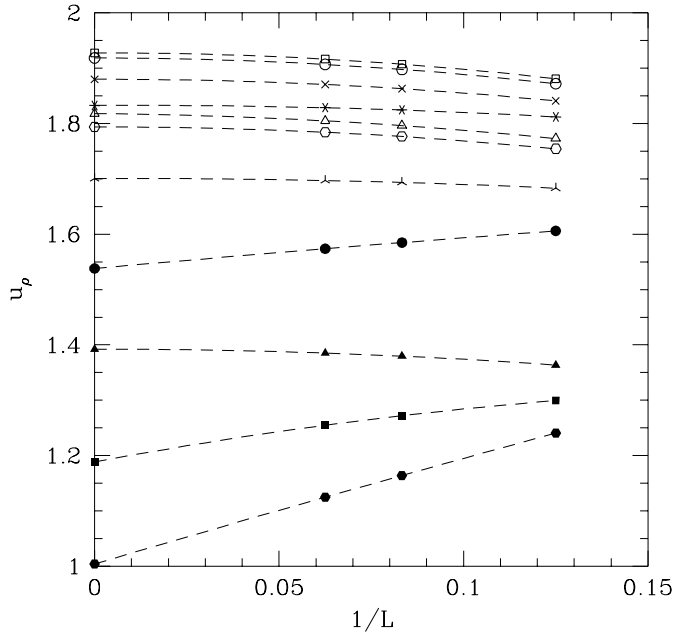

Figure 3.6: Size scaling of the charge velocity. Symbols as in Fig. 3.5.

Mean Field Theory with numerical diagonalization data, we briefly review the BCS equations for this model in arbitrary dimension for the choice $\beta = 0$ in Eq. (3.1). We also derive a closed expression for the critical value U_c^{BCS} which separates the superconducting ground state and the Luttinger (or Fermi) metal.

The interaction between Cooper pairs that arises from hamiltonian Eq.(3.1) is given by the effective potential:

$$V_{\mathbf{k}\mathbf{k}'} = U + 4\,\gamma \sum_{j=1}^{D} [\cos(k_j) + \cos(k'_j)] \ . \tag{3.39}$$

For $\gamma < 0$, $V_{\mathbf{k}\mathbf{k}'}$ at the Fermi level becomes less and less negative as particles are added. So we expect that superconductivity in this model, is favored at low density.

γ	U	K_ρ
0	4	0.71
0	8	0.62
-0.1	4	0.75
-0.1	8	0.64
-0.5	4	0.98
-0.5	8	0.78
-0.8	8	0.93

Table 3.1: Luttinger fixed point exponents.

γ	U	K_ρ
-0.1	0	1.07
-0.5	0	1.58
-0.8	0	1.78
-0.8	4	1.27

Table 3.2: Luther-Emery fixed point exponents.

The BCS equations are:

$$\begin{aligned}
\Delta_{\mathbf{k}} &= -\frac{1}{L^D}\sum_{\mathbf{k}'} V_{\mathbf{k}\mathbf{k}'}\,\frac{\Delta_{\mathbf{k}'}}{2E_{\mathbf{k}'}}\,,\\
E_{\mathbf{k}} &= \sqrt{(\tilde{\epsilon}_{\mathbf{k}}-\mu)^2+\Delta_{\mathbf{k}}^2}\,,\\
\tilde{\epsilon}_{\mathbf{k}} &= -2t\,(1-\frac{\gamma}{t}\mathrm{n})\sum_{j=1}^{D}\cos(k_j)\,,\\
\mathrm{n} &= 1-\frac{1}{L^D}\sum_{\mathbf{k}}\frac{\tilde{\epsilon}_{\mathbf{k}}-\mu}{E_{\mathbf{k}}}\,.
\end{aligned} \tag{3.40}$$

These equations coincide, with the identification (3.11) and

$$U \;\leftrightarrow\; U_1+\frac{3}{4}U_2-\frac{1}{2}\omega_0 g^2+\frac{7}{16}\omega_0 g^4$$

$$t \;\leftrightarrow\; t' \left(1 - \frac{g^4}{4}\,\mathrm{n}\right) ,$$

to the BCS equations obtained in Section 2.4 for the E–e Jahn–Teller hamiltonian in the weak coupling regime. This indicates that the superconducting phase of the two models is not only qualitatively but also quantitatively similar, moreover this equivalence is not restricted to the low density limit.

By following the same approach given in Section 2.4, it is easy to obtain an analytical expression for the critical line between the superconducting and the normal state:

$$U_c^{BCS}(\mathrm{n}) = \frac{4\gamma\mu}{t - \gamma\,\mathrm{n}} + \frac{2\,\gamma^2}{(t - \gamma\,\mathrm{n})^2} \int \frac{d^D\mathbf{k}}{(2\pi)^D}\, |\tilde{\epsilon}_{\mathbf{k}} - \mu| \,, \tag{3.41}$$

which coincides with the exact low density result (3.15) in the limit $n \to 0$. In fact, the BCS variational procedure becomes exact for two particles. Moreover, at weak coupling only the first term in (3.41) survives and the exact Renormalization Group result (3.36) is correctly reproduced. Notice that in BCS approximation the critical U does not vanish at half filling but tends to a finite limit which, in 1D, is $U_c(\mathrm{n}) = 8\gamma^2/\pi(t-\gamma)$. The model (3.1) and its Mean Field phase boundary (3.41) are defined in arbitrary dimension D and have a smooth limit for $D \to \infty$ provided both the hopping and the bond charge interaction are rescaled as $t \to t^*/(2D)^{1/2}$ and $\gamma \to \gamma^*/(2D)^{1/2}$ [1]. Due to the simple form of the density of states in the $D \to \infty$ limit, Eq. (3.41) can be analytically evaluated as:

$$U_c(\mathrm{n}) = \frac{2\gamma^*\mu^*}{t^*}\left[2 \;-\; \frac{\gamma^*(1-\mathrm{n})}{(t^* - \gamma^*\mathrm{n})}\right] \;+\; \frac{4\gamma^{*2}}{(t^* - \gamma^*\mathrm{n})}\frac{e^{-(\mu^*/t)^2/2}}{\sqrt{2\pi}} \,, \tag{3.42}$$

where the chemical potential μ^* is related to the density by

$$\mathrm{n} = 1 - \mathrm{erf}\left(\frac{-\mu^*}{t\sqrt{2}}\right) . \tag{3.43}$$

In Fig. 3.7 we show how the BCS phase boundary is modified when the dimensionality D grows from 1, 2, 3 to ∞. In particular, we notice that the critical U at zero density increases as $\sqrt{D}$ and, at $D = \infty$, the critical line has a singularity at $\mathrm{n} = 0$. As D increases, the superconducting region is pushed to lower densities but tends to a finite limit in the whole density axes up to $\mathrm{n} = 1$.

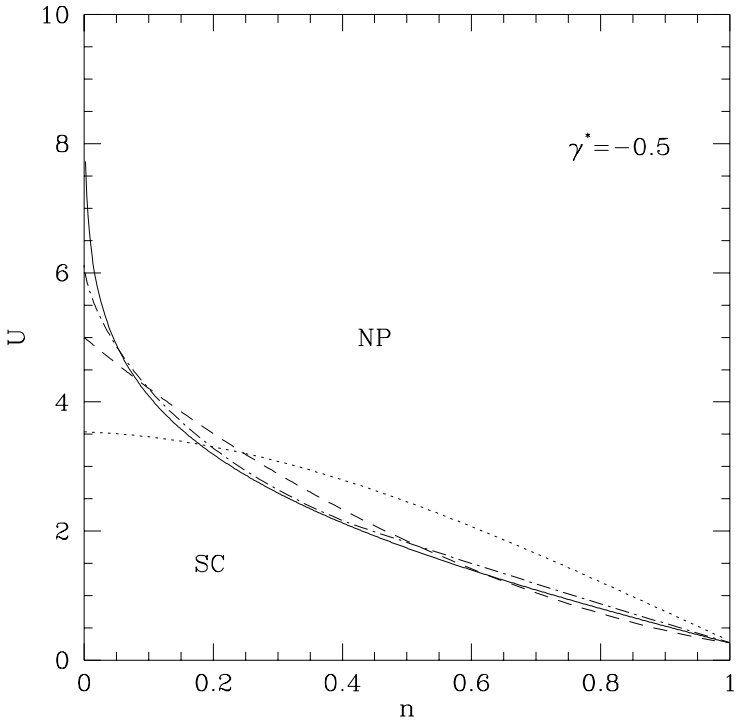

Figure 3.7: Mean Field phase boundary between a superconducting (SC) and a normal (NP) phase in BCS approximation for D=1 (dotted line), D=2 (dashed line), D=3 (dot-dash line) and $D = \infty$ (continuous line).

3.7 Phase diagram

In Fig. 3.8 we show the 1D zero temperature phase diagram in the (U, n) plane resulting from the combination of the various techniques reported before, for $\beta = 0$ and two different values of parameter γ. The solid line shows the phase boundary in Mean Field approximation, as obtained in the previous section. Its zero density limit is an exact result. Symbols represent numerical results at quarter filling obtained by finite size scaling of Lanczos diagonalizations. In particular, full circles correspond to the Luther Emery phase while open circles represent the Luttinger Liquid. The numerical data shown in these figures are quite

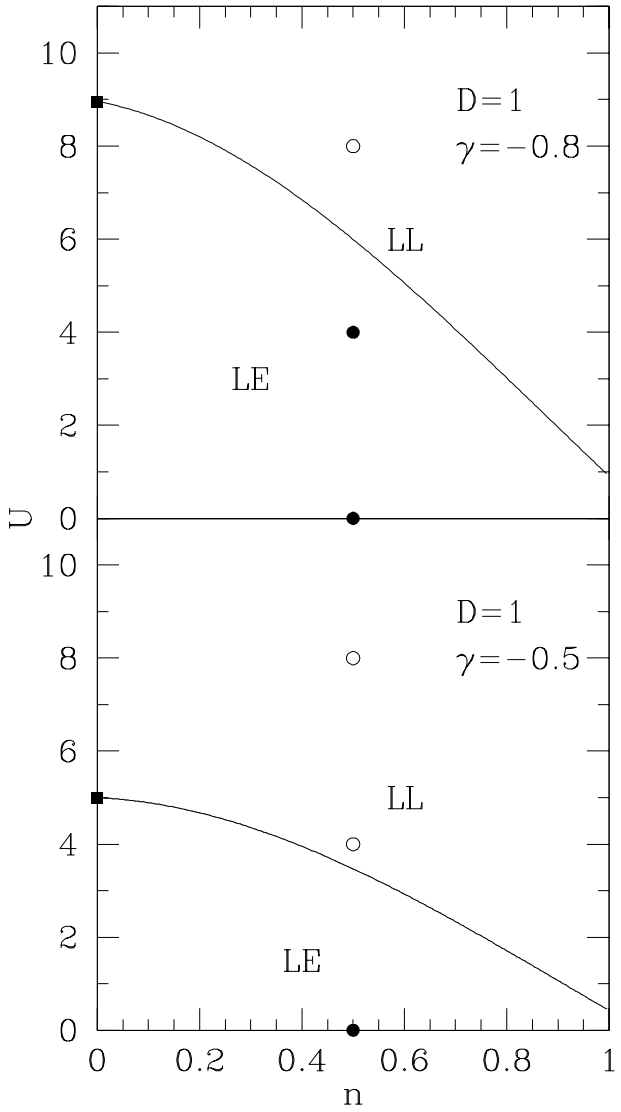

Figure 3.8: 1D phase diagram of the model 3.1 at zero temperature, for $\beta = 0$ and two choices of $\gamma < 0$. The continuous line is the BCS result separating a Luther Emery region (LE) form a Luttinger Liquid regimes (LL). The full square is the exact zero density limit. Circles are Lanczos results. Open symbols correspond to the Luttinger Liquid. Full circles to the Luther Emery phase.

consistent with the Mean Field estimate of the critical line, giving confidence to the BCS variational procedure for this class of systems.

The 2D model can be studied both within Mean Field Theory and by Lanczos diagonalizations. The critical line in BCS approximation has been obtained in the previous section and is shown in Fig. 3.9 for $\beta = 0$ and two choices of γ. Again we remark that the zero density limit is an exact result and coincides with what has been found via the two–particle analysis. Mean Field Theory predicts a non–zero critical U_c also at half filling. The superconducting region, below the critical line, has a spin gap and true (off–diagonal) long range order, while above the critical line the model is in a Fermi Liquid regime. In order to test this Mean Field phase diagram, we have carried out Lanczos diagonalizations also in the 2D model. In this case, however, a finite size scaling of the results is not possible, due to the exceedingly large Hilbert space dimensions and our analysis is limited to a 4×4 lattice. The results of the numerical analysis at quarter filling are shown in the same figure by full circles if the system turns out to be in the superconducting region and by open dots if it is a Fermi liquid. The method we have used for extracting this information from the diagonalization data is quite similar to the one adopted in one dimension. The 4×4 lattice with 8 electrons, zero magnetization and periodic boundary conditions is 16 times degenerate in the non interacting case ($U = \gamma = 0$). However, interactions split this degeneracy favoring some of the zero momentum states: The positive U Hubbard model has a singlet ground state with d–wave symmetry [67] while a BCS superconducting state is expected to have s–wave symmetry. Therefore, a level crossing between these two (spatial) symmetries would suggest a change in the physical nature of the ground state, i.e. the crossing of the phase boundary between a Fermi liquid and a superconductor. Other, more conventional, methods for investigating the properties of the state, like the study of the spin gap or the analysis of the correlation functions, are strongly affected by the limitations in the lattice size and require a careful size scaling in order to give reliable results.

The symmetry based analysis lead us to the identification of the phases of the model for different choices of the parameters. The results, shown in Fig. 3.9 compare rather favor-

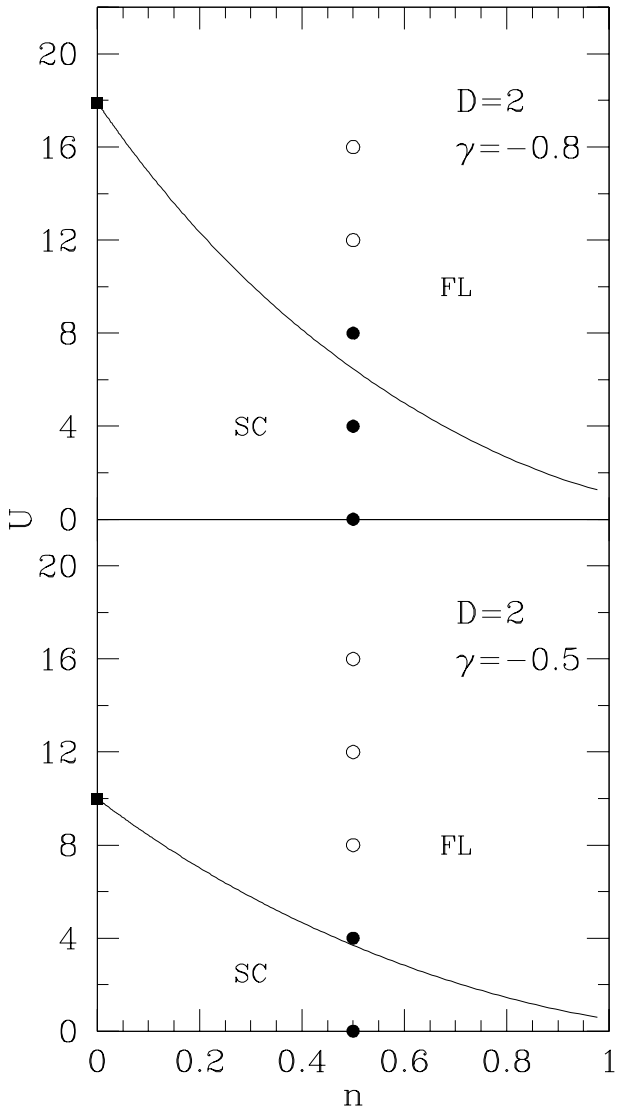

Figure 3.9: 2D phase diagram. Notation as in Fig. 3.8. Here the two phases represent a superconductor (SC) and a Fermi liquid (FL).

ably with the BCS variational predictions, supporting the existence of a phase transition between a superconducting and a Fermi liquid phase in the 2D model at finite density. The character of the superconductive phase will probably change smoothly with increasing density, going from a dimer gas at low density to a regime of weakly bound Cooper pairs, similar to the usual BCS picture.

Conclusions

In this thesis we have considered and studied some models of strongly correlated electron systems, whose interest has been revived in condensed matter since the discovery of high temperature cuprate and fulleride superconductors.

In the first Chapter we have proposed and studied the infinite dimensional limit of the repulsive Hubbard model on a class of non–nested bipartite lattices which generalize the two–dimensional honeycomb and three–dimensional diamond lattice, and are characterized by a semi-metallic non-interacting density of states. As for the hyper–cubic case, the problem reduces to a single–impurity Anderson model supplemented by a self–consistency condition. Using Monte Carlo simulations and second–order perturbation theory we have determined the complete phase diagram of the model at half–filling. It shows a non-magnetic semi-metallic region and an antiferromagnetic insulating phase with a critical value of U for the transition at $T = 0$ which is strictly positive, $U_c/t \approx 2.3$, in contrast with the hypercubic lattice, where antiferromagnetic order sets in at $U_c = 0$. The Mott–Hubbard transition, which we have found at $U_{MH}/t \approx 8.5$, is not a true ground–state phase transition, but just a transition occurring within the paramagnetic solution continued to a region of the phase diagram where it becomes actually unstable towards the antiferromagnetic insulating solution. In this respect, the situation is similar to the regular hyper–cubic lattice.

In the second and third Chapter we have focused our attention on some new possible mechanisms proposed to explain superconductivity in fullerides and oxides.

More precisely, in Chapter2 we have studied a model with two degenerate electronic molecular states coupled to a doubly degenerate optical phonon both in the weak and in the strong electron–phonon coupling limit. We have shown that, as a consequence of the orbital degeneracy, a new tendency to electron paring appears. This effect, which is completely absent in the non-degenerate case, may lead to superconductivity even when the electronic repulsion overcomes the standard polaronic attraction.
The exact two–particle solution and the BCS solution shows that the contribution to superconductivity coming from the orbital degeneracy has advantages with respect to the on–site polaronic attraction, for instance it is robust to the presence of local repulsion and it takes advantage by a larger coordination number. However its strength is much smaller, at least in the weak and in the strong coupling limit we have analyzed, than the on–site polaronic term, so that it is still an open question whether it may play a relevant role as a mechanism for phonon-induced superconductivity.
In the zero density limit we have provided a common physical picture for the ground state of the system both in the weak and in the strong coupling regime. At higher density however the strong coupling version of the model could only be analyzed numerically and in one dimension [24]. On the other hand most of the interesting features which are found in the strong electron–phonon coupling limit, are already present in the weak coupling regime. This because the modification of the degeneracy of the molecular levels according to the electronic occupancy, which is at the origin of extra–pairing phenomenon, is preempted by the electron–phonon interaction in the strong as well as in the weak coupling regime. Moreover the weak coupling limit has in addition the big advantage of allowing a more systematic analytical approach (e.g. BCS solution), valid in any dimension.

In Chapter 3 we have studied a simple tight binding model characterized by on–site Hubbard repulsion and nearest neighbor bond–charge interaction. This model is of interest on its own, since a bond hopping term can appear as a correlation effect due to tracing out other spectator electrons present on each site. However, we can also recover this model in connection with the electron–vibron problem considered in Chapter 2. In fact we have shown

that the bond–charge hamiltonian can be regarded as an *effective* one–band hamiltonian for the E–e model, at least for the superconducting region of the phase diagram.

We have presented analytical and numerical results both in one and two dimension showing the presence of a phase transition at zero temperature between a superconducting region at small U and a Fermi liquid regime at larger repulsions. Superconductivity is rather insensitive to Hubbard U due to the the *off diagonal* nature of the interaction responsible for binding. In 1D the analysis is much more rigorous due to the many powerful tools available, including weak coupling Renormalization Group and conformal field theory. In the 1D case the phase transition occurs between a Luther Emery regime (quasi superconducting) and a Luttinger Liquid phase (quasi Fermi liquid). The correlation exponents and a quantitative characterization of the different phases are obtained by use of Lanczos diagonalizations combined with field theoretical techniques. A BCS variational analysis is in good agreement with the exact results presented in this work and reproduces the main features of the zero temperature phase diagram. The analytical study of the few particle problem leads to a physical picture of the superconductive phase in terms of a superfluid dimer gas both in one and two dimensions and, in 1D, allows for the quantitative evaluation of the correlation exponents in the zero density limit.

Appendix A

$D = \infty$. Reduction to a local problem

In this section we will sketch the argument which allows to write the local Green's function as the self-consistent solution of a local problem. There are many possible approaches to get to the final result. Our proof is based on the ideas contained in Ref. [8].

The starting point is the Dyson equation for the Green's function. Due to the locality in space of the self-energy function ($\Sigma(i,j) = 0$ for $i \neq j$) we can clearly write

$$G_\sigma(i,j) = G^o_\sigma(i,j) + \sum_l G^o_\sigma(i,l)\,\Sigma_\sigma(l,l)\,G_\sigma(l,j)\,. \tag{A.1}$$

Let us now define an auxiliary Green's function $\mathcal{G}^o_\sigma(i,j)$ which satisfies a similar Dyson equation with a restriction in the lattice sum as follows:

$$\mathcal{G}^o_\sigma(i,j) = G^o_\sigma(i,j) + \sum_{l\neq j} G^o_\sigma(i,l)\,\Sigma_\sigma(l,l)\,\mathcal{G}^o_\sigma(l,j)\,. \tag{A.2}$$

In other words, $\mathcal{G}^o_\sigma(i,j)$ embodies the correlation effects due to the medium around the site under consideration.

Our first goal is to show that the local Green's function $G_\sigma(i,i)$ satisfies a *local* Dyson equation where the non–interacting propagator G^o is formally replaced by the auxiliary

Green's function $\mathcal{G}^o_\sigma(i,i)$:

$$G_\sigma(i,i) = \mathcal{G}^o_\sigma(i,i) + \mathcal{G}^o_\sigma(i,i)\,\Sigma_\sigma(i,i)\,G_\sigma(i,i)\,. \tag{A.3}$$

We start by iterating Eq. (A.2) to get a series of the form

$$\begin{aligned}\mathcal{G}^o_\sigma(i,j) &= G^o_\sigma(i,j) + \sum_{l_1\neq j} G^o_\sigma(i,l_1)\,\Sigma_\sigma(l_1,l_1)\,G^o_\sigma(l_1,j) + \cdots \\ &= G^o_\sigma(i,j) + \sum_{n=1}^{\infty}\sum_{l_1\neq j}\sum_{l_2\neq j}\cdots\sum_{l_n\neq j} G^o_\sigma(i,l_1)\,\Sigma_\sigma(l_1,l_1)\cdots\Sigma_\sigma(l_n,l_n)\,G^o_\sigma(l_n,j)\,.\end{aligned} \tag{A.4}$$

Clearly, iterating the full Dyson equation for $G_\sigma(i,j)$ generates a similar formal expansion with the only difference that the restriction in the lattice sums in Eq. (A.4) is completely removed.

Consider now carrying out the same formal expansion for the local Dyson equation we are trying to establish, Eq. (A.3),

$$\begin{aligned}G_\sigma(i,i) &= \mathcal{G}^o_\sigma(i,i) + \mathcal{G}^o_\sigma(i,i)\,\Sigma_\sigma(i,i)\,\mathcal{G}^o_\sigma(i,i) + \cdots \\ &= \mathcal{G}^o_\sigma(i,i) + \sum_{n=1}^{\infty} \mathcal{G}^o_\sigma(i,i)\,\Sigma_\sigma(i,i)\cdots\Sigma_\sigma(i,i)\,\mathcal{G}^o_\sigma(i,i)\,,\end{aligned} \tag{A.5}$$

and substituting the series in Eq. (A.4) (with $i = j$) for each occurrence of $\mathcal{G}^o_\sigma(i,i)$ in Eq. (A.5). Let us now regroup all the terms in Eq. (A.5) with the same number of Σ. The zero-th order term is clearly $G^o_\sigma(i,i)$. To see how things work for higher order terms, consider all the contributions with *one* Σ only. Clearly, these can only be originated from the first and second terms in the right hand side of Eq. (A.5), and read

$$\begin{aligned}[\text{Terms with one } \Sigma] &= \sum_{l_1\neq i} G^o_\sigma(i,l_1)\,\Sigma_\sigma(l_1,l_1)\,G^o_\sigma(l_1,i) + G^o_\sigma(i,i)\,\Sigma_\sigma(i,i)\,G^o_\sigma(i,i) \\ &= \sum_{l_1} G^o_\sigma(i,l_1)\,\Sigma_\sigma(l_1,l_1)\,G^o_\sigma(l_1,i)\,,\end{aligned} \tag{A.6}$$

i.e. the unrestricted lattice sum appearing in the formal expansion of $G_\sigma(i,i)$ is recovered. Similarly, by focusing on all the terms with n appearances of Σ, we realize that all the restrictions in the lattice sums are removed and we get the formal expansion for the local Green's function, which concludes the argument.

Reducing the calculation of $G_\sigma(i,i)$ to the local problem in Eq. (A.3) is the big simplification achieved in infinite dimensions due to the locality of the self-energy. One can in principle use all the tools developed to treat a single–impurity Anderson problem, except that we still lack of a prescription for calculating the auxiliary local Green's function $\mathcal{G}^o_\sigma(i,i)$. To close the loop, we consider once again the full Dyson equation for G, this time in $\mathbf{k}$-space. It reads:

$$\hat{G}_\sigma(\mathbf{k}) \;=\; ([\hat{G}^o_\sigma(\mathbf{k})]^{-1} \;-\; \hat{\Sigma}_\sigma)^{-1} \tag{A.7}$$

where we have used a 2×2 matrix notation to treat the various components $(AA, AB, ...)$ in a compact way. The local Green's function, on the other hand, is simply given by the sum over the Brillouin zone of the appropriate component of $\hat{G}_\sigma(\mathbf{k})$, i.e.

$$\begin{aligned} G_\sigma(i,i) &= \frac{1}{N}\sum_{\mathbf{k}}^{BZ}[\hat{G}_\sigma(\mathbf{k})]_{\alpha\alpha} \\ &= \frac{1}{N}\sum_{\mathbf{k}}^{BZ}\left[[(\hat{G}^o_\sigma(\mathbf{k}))^{-1} \;-\; \hat{\Sigma}_\sigma]^{-1}\right]_{\alpha\alpha} , \end{aligned} \tag{A.8}$$

where the symbol α stands for the sublattice ($\alpha = A$ or B) to which site i belongs. An explicit calculation shows that the dependence on $\mathbf{k}$ of the right hand side of Eq. (A.8) is contained exclusively in the band energy $E_{\mathbf{k}}$, allowing us to rewrite the sum over $\mathbf{k}$ into an integral involving the non–interacting density of states $\rho(E)$. Explicitly, after some simple algebra one arrives at

$$G_{\alpha\sigma}(\omega_n) \;\equiv\; G_\sigma(i,i)(\omega_n) \;=\; \int_0^\infty dE\; \rho(E)\, \frac{Z^{\bar{\alpha}}_\sigma}{Z^A_\sigma Z^B_\sigma - E^2} , \tag{A.9}$$

where

$$Z^\alpha_\sigma \;=\; i\omega_n + \mu + (-1)^R \sigma H_S - \Sigma_{\alpha\sigma}(\omega_n) , \tag{A.10}$$

and $\bar{\alpha}$ denotes sublattice B is $\alpha = A$ and viceversa. Notice that in the above equations we have allowed for the presence of a staggered magnetic field H_S which is useful to calculate the staggered susceptibilty of the system using only single–particle quantities.

Eqs. (A.3,A.9) are the required relations which allow us to solve the problem *iteratively* given a method for calculating Σ_σ from a fictitious non-interacting $\mathcal{G}^o$, as explained in the text.

Bibliography

[1] W. Metzner and D. Vollhardt, Phys. Rev. Lett. **62**, 324 (1989). For a review see, for instance, D. Vollhardt, Physica B **169**, 277 (1991).

[2] H. Schweitzer and G. Czycholl, Solid State Comm. **69**, 171 (1989).

[3] U. Brandt and C. Mielsch, Z. Phys. B **75**, 365 (1989).

[4] See, for instance, T. Kennedy, E. H. Lieb and B. H. Shastry, Phys. Rev. Lett. **61**, 2582 (1988).

[5] P. van Dongen, F. Gebhard and D. Vollhardt, Z. Phys. B **76**, 197 (1989).

[6] F. Gebhard, Phys. Rev. B **41**, 9452 (1990).

[7] A. Georges and G. Kotliar, Phys. Rev. B **45**, 6479 (1992).

[8] M. Jarrell, Phys. Rev. Lett. bf 69, 168 (1992). See also T. Pruschke, D. L. Cox, and M. Jarrell, Phys. Rev. B **47**, 3553 (1993).

[9] M. J. Rozenberg, X. Y. Zhang, and G. Kotliar, Phys. Rev. Lett. **69**, 1236 (1992).

[10] A. Georges and W. Krauth, Phys. Rev. Lett. **69**, 1240 (1992).

[11] G. Santoro, M. Airoldi, S. Sorella and E. Tosatti, Phys. Rev. B **47**, 16216 (1993).

[12] S. Sorella and E. Tosatti, Europhys. Lett. **19**, 699 (1992).

[13] N. F. Mott, Phil. Mag. **6**, 287 (1961).

[14] J. Hubbard, Proc. Roy. Soc. (London) A **281**, 401 (1964).

[15] W. F. Brinkman and T. M. Rice, Phys. Rev. B **2**, 4302 (1970).

[16] A. Georges and W. Krauth, Phys. Rev. B **48**, 7167 (1993).

[17] A model on a fully connected lattice with randomness in the hopping parameters which completely inhibits AF long range order has been discussed in the literature, see Ref. [31] in Ref. [16].

[18] R. Englman, The Jahn–Teller Effect in Molecules and Crystals, Wiley–Interscience, New York, 1973.

[19] I.B. Bersuker and V.Z. Polinger, Vibronic Interactions in Molecules and Crystals, Springer Verlag, Berlin, 1989.

[20] A. Auerbach, Phys. Rev. Lett. **72**, 2931 (1994); A. Auerbach, N. Manini and E. Tosatti, Phys. Rev. B **49**, 12998 (1994); N. Manini, E. Tosatti and A. Auerbach, *ibid* **49**, 13008 (1994).

[21] O. Gunnarsson, Phys. Rev. Lett. **51**, 3493 (1995).

[22] N. Manini and E. Tosatti, preprint (1995).

[23] N. Manini, E. Tosatti and S. Doniach, Phys. Rev. B **51**, 3731 (1995).

[24] G. Santoro, M. Airoldi, N. Manini, E. Tosatti and A. Parola, Phys. Rev. Lett. **74**, 4039 (1995).

[25] M. Fabrizio, M. Airoldi and E. Tosatti, submitted to Phys. Rev. B (1995).

[26] K. I. Kugel and D.I. Khomskii, Sov. Phys. Usp. **25(4)**, 231 (1982).

[27] G. A. Gehring and K. A. Gehring, Rep. Prog. Phys. **38**, 1 (1975).

[28] G. Santoro, A. Parola and E. Tosatti (unpublished)

[29] See for instance V.J. Emery in: Highly Conducting One Dimensional Solids, J.T. De Vreese, R.P. Evrard, V.E. Van Doren (eds.), Plenum, N.Y. (1979).

[30] M. Ogata, M.U. Luchini, S. Sorella and F.F. Assaad, Phys. Rev. Lett. **66**, 2388 (1991).

[31] M. Grilli, R. Raimondi, C. Castellani, C. Di Castro and G. Kotliar, Phys. Rev. Lett. **67**, 259 (1991).

[32] E. Dagotto *et al*, Phys. Rev. B **49**, 3548 (1994).

[33] F.B. Essler, V.E. Korepin and K. Schoutens, Phys. Rev. Lett. **68**, 2960 (1992); J. de Boer, V.E. Korepin and A. Schadschneider, ITP preprint (1994).

[34] R.Z. Bariev, A. Klümper, A. Schadschneider and J. Zittartz, J. Phys. A:Math. Gen. **26**, 1249 (1993).

[35] J.E. Hirsch and F. Marsiglio, Phys. Rev. B **39**, 11515 (1989).

[36] J.E. Hirsch and F. Marsiglio, Physica C **162-164**, 591-596 (1989).

[37] F. Marsiglio and J.E. Hirsch, Phys. Rev. B **41**, 6435 (1989).

[38] J.E. Hirsch, Physica C **158**, 326 (1989); Phys. Letters A **138**, 83 (1989).

[39] J. Hubbard, Proc. Roy. Soc. (London) A **276**, 238 (1963).

[40] R. Micnas, J. Ranninger and S. Robaszkiewicz, Phys. Rev. B **39**, 11653 (1989).

[41] J.E. Hirsch, Physica B **199–200**, 366 (1994).

[42] F. Guinea, Physica C **153–155**, 1231 (1988).

[43] J.E. Hirsch and F. Marsiglio, Phys. Rev. B **41**, 2049 (1990).

[44] J.E. Hirsch, Phys. Rev. B **43**, 11400 (1991).

[45] M.E. Simon and A.A. Aligia, Phys. Rev. B **48**, 7471 (1993).

[46] J.E. Hirsch, Phys. Rev. B **47**, 5351 (1993); F. Marsiglio and J.E. Hirsch, Phys. Rev. B **49**, 1366 (1994).

[47] M. Airoldi and A. Parola, Phys. Rev. B **51**, 16327 (1995).

[48] E. Müller-Hartmann, Z. Phys. B **74**, 507 (1989)

[49] A. Georges, G. Kotliar and Q. Si, Int. J. Mod. Phys. B **6**, 705 (1992).

[50] J. E. Hirsch and R. M. Fye, Phys. Rev. Lett. **56**, 2521 (1986).

[51] N. E. Bickers and S. R. White, Phys. Rev. B **43**, 8044 (1991).

[52] A rationale for the good results provided by the IPT for the particle-hole symmetric case has been presented by X. Y. Zhang, M. J. Rozenberg and G. Kotliar, Phys. Rev. Lett. **70**, 1666 (1993). It is based on the observation that both the $U = 0$ limit and the $t = 0$ (atomic) limit are correctly reproduced by the second order approximation for Σ.

[53] Wagner, M., Unitary Transformation Methods in Vibronic Problems, North–Holland, Amsterdam, 1984.

[54] A. Parola *et al.* in "Proc. Nato Advanced Research Workshop on Dynamics of Magnetic Fluctuations in High Temperature Superconductors", ed G. Reiter, P. Horsch and G. Psaltakis (N.Y. Plenum 1990).

[55] B. Sutherland, Phys. Rev. B **12**, 3795 (1975)

[56] I. Affleck, Phys. Rev. Lett. **54**, 966 (1985).

[57] R. Strack and D. Vollhardt, Phys. Rev. Lett. **70**,2637 (1993).

[58] L. Arrachea and A.A. Aligia, Phys. Rev. Lett. **73**, 2240 (1994).

[59] F. Marsiglio and J.E. Hirsch, Physica C **171**, 554-560 (1990).

[60] The quadratic dependence of the energy as a function of the total momentum P holds for a finite number of particles in vacuum while, at finite density, a term linear in P is also present. This contribution, which vanishes linearly with the number density n in 1D, is expected in a hard core dimer gas.

[61] H. Frahm and V.E. Korepin Phys. Rev. B **42**, 10553 (1990); H. Schulz, Int. J. Mod. Phys. **5**, 57 (1991).

[62] J. Sólyom, Adv. Phys. **28**, 201 (1979).

[63] F.D.M. Haldane, J. Phys. C **14**, 2585 (1981); H. Schulz, Phys. Rev. Lett. **64**, 2831 (1990).

[64] G. Japaridze and E. Müller-Hartmann, Ann. Physik **3**, 163-180 (1994).

[65] M. Ogata and H. Shiba, Phys. Rev. B **41**, 2326 (1990).

[66] S. Sorella, A. Parola, M. Parrinello and E. Tosatti, Europhys. Lett. **12**, 721 (1990).

[67] A. Parola, S. Sorella, M.Parrinello and E.Tosatti, Phys. Rev. B, **43**, 6190, (1991).